

COUPLING STOKES–DARCY FLOW WITH TRANSPORT*

DANAIL VASSILEV[†] AND IVAN YOTOV[†]

Abstract. A mathematical and numerical model describing chemical transport in a Stokes–Darcy flow system is discussed. The flow equations are solved through domain decomposition using classical finite element methods in the Stokes region and mixed finite element methods in the Darcy region. The local discontinuous Galerkin (LDG) method is used to solve the transport equation. Models dealing with coupling between Stokes and Darcy equations have been extensively discussed in the literature. This paper focuses on the approximation of the transport equation. Stability of the LDG scheme is analyzed, and an a priori error estimate is proved. Several numerical examples verifying the theory and illustrating the capabilities of the method are presented.

Key words. Stokes–Darcy flow, coupled flow and transport, error estimates, local discontinuous Galerkin

AMS subject classifications. 65M12, 65M15, 65N30, 76D07, 76S05

DOI. 10.1137/080732146

1. Introduction. Coupling the Stokes and Darcy equations has become a very active area of research because of its potential for practical applications. Such models can be used to describe physiological phenomena like the blood motion in vessels, hydrological systems in which surface water percolates through rocks and sand, and various industrial processes involving filtration. One serious problem today is surface water and groundwater contamination resulting from leaky underground storage tanks, chemical spills, and various human activities. A model coupling the Stokes–Darcy equations with a transport equation can be used to study the spread of pollution released in the water and assess the danger.

There are a number of stable and convergent numerical methods developed for the coupled Stokes–Darcy flow system; see, e.g., [24, 21, 25, 28, 22]. We will concentrate on the methods developed in [24, 28]. Both methods utilize a mixed finite element (MFE) method in the porous media domain, which computes the velocity directly and with high accuracy. Also, MFE methods provide locally mass conservative velocities, a property critical for the transport problem in order to avoid creating artificial mass sources and sinks. The method developed in [28] is especially suited for coupling with transport since there a discontinuous Galerkin (DG) approximation is used for the Stokes equation, giving locally mass conservative velocities in the Stokes region as well.

This paper studies the coupling of the Stokes–Darcy flow system with an advection-diffusion equation that models transport of a chemical. For the numerical approximation of the transport problem we employ the local discontinuous Galerkin (LDG) method [15, 13], which conserves mass locally and approximates sharp fronts accurately. The method can be defined on general grids and allows one to vary the degree of the approximating polynomial space from element to element. The LDG method can be thought of as a discontinuous MFE method since it approximates

*Received by the editors August 4, 2008; accepted for publication (in revised form) June 16, 2009; published electronically October 1, 2009. This work was partially supported by the NSF grants DMS 0620402 and DMS 0813901 and the DOE grant DE-FG02-04ER25618.

<http://www.siam.org/journals/sisc/31-5/73214.html>

[†]Department of Mathematics, University of Pittsburgh, 301 Thackeray Hall, Pittsburgh, PA 15260 (dhv1@pitt.edu, yotov@math.pitt.edu).

both the concentration and the diffusive flux. Primal DG discretizations of advection-diffusion equations have also been studied [31] and could be applied to our problem. For the sake of space we limit our presentation to LDG discretizations. Couplings of Darcy flow with DG approximations for transport have been studied in [30, 19].

In this paper we develop stability and convergence analysis for the concentration and the diffusive flux in the transport equation. The numerical error is a combination of the LDG discretization error and the error from the discretization of the Stokes–Darcy velocity. The former is shown to be of the order $O(h^k)$, where k is the polynomial degree in the LDG approximating space. This is similar to existing bounds in the literature for stand-alone LDG discretizations [15, 13, 10]. The error terms coming from the Stokes–Darcy flow discretization are of optimal order, similar to the bounds obtained in [24, 28]. This is an improvement of $O(h)$ from the result in [20], where the Darcy velocity discretization error is incorporated into the error analysis of an LDG method for the transport equation. We also extend previous LDG transport analysis [15, 20, 10, 13] to nondivergence free velocity.

The rest of the paper is organized as follows. In section 2 we present the model flow-transport problem. The Stokes–Darcy flow discretization and the LDG transport discretization are given in sections 3 and 4, respectively. Section 5 is devoted to the stability of the LDG scheme. The error analysis of the LDG method is presented in section 6. The paper ends with numerical experiments in section 7.

2. Model problem. In our model we consider a fluid region $\Omega_1 \subset \mathbb{R}^d$, $d = 2, 3$, in which the flow is governed by the Stokes equations (2.1)–(2.3) and a porous medium $\Omega_2 \subset \mathbb{R}^d$ in which Darcy’s law (2.4)–(2.6) holds. The two regions are separated by an interface Γ_{12} through which the fluid can flow in both directions. We assume that the subdomains are polygonal for $d = 2$ or polyhedral for $d = 3$. Let \mathbf{n}_i be the outward unit normal vector to $\partial\Omega_i$, $i = 1, 2$, let $\boldsymbol{\tau}_j$, $j = 1, d - 1$, be an orthonormal system of tangential vectors on Γ_{12} , and let $\Gamma_i := \partial\Omega_i \setminus \Gamma_{12}$. Let $\mathbf{u}_i : \Omega_i \rightarrow \mathbb{R}^d$ and $p_i : \Omega_i \rightarrow \mathbb{R}$ denote, respectively, the velocity and the pressure in Ω_i . Let $\mathbf{De}(\mathbf{u}_1)$ and $\mathbf{T}(\mathbf{u}_1, p_1)$ denote, respectively, the deformation rate tensor and the stress tensor:

$$\mathbf{De}(\mathbf{u}_1) = \frac{1}{2}(\nabla\mathbf{u}_1 + \nabla\mathbf{u}_1^T), \quad \mathbf{T}(\mathbf{u}_1, p_1) = -p_1\mathbf{I} + 2\mu\mathbf{De}(\mathbf{u}_1),$$

where μ is the fluid viscosity. Let $\mathbf{f}_1 \in (L^2(\Omega_1))^d$ be the body force in Ω_1 , and let $\mathbf{g}_1 \in (H^{1/2}(\Gamma_1))^d$ be the boundary velocity data. In Ω_2 , \mathbf{K} is a symmetric and positive definite rock permeability tensor with components bounded from above, $\mathbf{f}_2 \in (L^2(\Omega_2))^d$ represents the gravity force, $q_2 \in L^2(\Omega_2)$ is a source (sink) function satisfying the solvability condition (2.7), and $g_2 \in L^2(\Omega_2)$ is the boundary normal velocity data. In addition we also assume that on Γ_{12} the interface conditions (2.8)–(2.10) are satisfied. The flow model is

$$(2.1) \quad -\nabla \cdot \mathbf{T} \equiv -2\mu\nabla \cdot \mathbf{De}(\mathbf{u}_1) + \nabla p_1 = \mathbf{f}_1 \quad \text{in } \Omega_1,$$

$$(2.2) \quad \nabla \cdot \mathbf{u}_1 = 0 \quad \text{in } \Omega_1,$$

$$(2.3) \quad \mathbf{u}_1 = \mathbf{g}_1 \quad \text{on } \Gamma_1,$$

$$(2.4) \quad \mu\mathbf{K}^{-1}\mathbf{u}_2 + \nabla p_2 = \mathbf{f}_2 \quad \text{in } \Omega_2,$$

$$(2.5) \quad \nabla \cdot \mathbf{u}_2 = q_2 \quad \text{in } \Omega_2,$$

$$(2.6) \quad \mathbf{u}_2 \cdot \mathbf{n}_2 = g_2 \quad \text{on } \Gamma_2,$$

$$(2.7) \quad \int_{\Omega_2} q_2 \, d\mathbf{x} = \int_{\Gamma_1} \mathbf{g}_1 \cdot \mathbf{n}_1 \, d\sigma + \int_{\Gamma_2} g_2 \, d\sigma,$$

$$(2.8) \quad \mathbf{u}_1 \cdot \mathbf{n}_1 + \mathbf{u}_2 \cdot \mathbf{n}_2 = 0 \quad \text{on } \Gamma_{12},$$

$$(2.9) \quad -\mathbf{n}_1 \cdot \mathbf{T} \cdot \mathbf{n}_1 \equiv p_1 - 2\mu \mathbf{n}_1 \cdot \mathbf{De}(\mathbf{u}_1) \cdot \mathbf{n}_1 = p_2 \quad \text{on } \Gamma_{12},$$

$$(2.10) \quad -\frac{\sqrt{K_j}}{\mu\alpha} \mathbf{n}_1 \cdot \mathbf{T} \cdot \boldsymbol{\tau}_j \equiv -\frac{\sqrt{K_j}}{\alpha} 2\mathbf{n}_1 \cdot \mathbf{De}(\mathbf{u}_1) \cdot \boldsymbol{\tau}_j = \mathbf{u}_1 \cdot \boldsymbol{\tau}_j, \quad j = 1, d - 1, \text{ on } \Gamma_{12}.$$

Conditions (2.8) and (2.9) impose continuity of flux and normal stress, respectively. Condition (2.10) is known as the Beavers–Joseph–Saffman law [5, 29], where $K_j = \boldsymbol{\tau}_j \cdot \mathbf{K} \cdot \boldsymbol{\tau}_j$ and $\alpha > 0$ is an experimentally determined dimensionless constant.

The Stokes–Darcy flow system is coupled with the transport equation on $\Omega = \Omega_1 \cup \Omega_2$:

$$(2.11) \quad \phi c_t + \nabla \cdot (\mathbf{c}\mathbf{u} - \mathbf{D}\nabla c) = \phi s \quad \forall (\mathbf{x}, t) \in \Omega \times (0, T),$$

where $c(\mathbf{x}, t)$ is the concentration of some chemical component, $0 < \phi_* \leq \phi(\mathbf{x}) \leq \phi^*$ is the porosity of the medium in Ω_2 (it is set to 1 in Ω_1), $\mathbf{D}(\mathbf{x}, t)$ is the diffusion/dispersion tensor assumed to be symmetric and positive definite with smallest and largest eigenvalues D_* and D^* , respectively, $s(\mathbf{x}, t)$ is a source term, and \mathbf{u} is the velocity field defined by $\mathbf{u}|_{\Omega_i} = \mathbf{u}_i$, $i = 1, 2$. The model is completed by the initial condition

$$(2.12) \quad c(\mathbf{x}, 0) = c^0(\mathbf{x}), \quad \forall \mathbf{x} \in \Omega$$

and the boundary conditions

$$(2.13) \quad (\mathbf{c}\mathbf{u} - \mathbf{D}\nabla c) \cdot \mathbf{n} = (c_{in}\mathbf{u}) \cdot \mathbf{n} \quad \text{on } \Gamma_{in},$$

$$(2.14) \quad (\mathbf{D}\nabla c) \cdot \mathbf{n} = 0 \quad \text{on } \Gamma_{out}.$$

Here, $\Gamma_{in} := \{\mathbf{x} \in \partial\Omega : \mathbf{u} \cdot \mathbf{n} < 0\}$, $\Gamma_{out} := \{\mathbf{x} \in \partial\Omega : \mathbf{u} \cdot \mathbf{n} \geq 0\}$, and \mathbf{n} is the unit outward normal vector to $\partial\Omega$. We will also use the notation $\Gamma = \partial\Omega$.

Throughout the paper K will denote a generic constant independent of the discretization parameters h_1 , h_2 , and h . We will use the following standard notation. For a domain $G \subset \mathbb{R}^d$, the $L^2(G)$ inner product and norm for scalar and vector valued functions are denoted by $(\cdot, \cdot)_G$ and $\|\cdot\|_G$, respectively. The norms and seminorms of the Sobolev spaces $W^{k,p}(G)$, $k \in \mathbb{R}$, $p > 0$, are denoted by $\|\cdot\|_{k,p,G}$ and $|\cdot|_{k,p,G}$, respectively. The norms and seminorms of the Hilbert spaces $H^k(G)$ are denoted by $\|\cdot\|_{k,G}$ and $|\cdot|_{k,G}$, respectively. We omit G in the subscript if $G = \Omega$. For a section of the domain or element boundary $S \subset \mathbb{R}^{d-1}$ we write $\langle \cdot, \cdot \rangle_S$ and $\|\cdot\|_S$ for the $L^2(S)$ inner product (or duality pairing) and norm, respectively.

3. Stokes–Darcy flow discretization. Let $\mathcal{T}_{h,i}$ be a shape-regular affine finite element partition of Ω_i [12] with a maximum element diameter h_i , $i = 1, 2$. We allow for the traces of the grids on Γ_{12} to be nonmatching and assume that no point of the interface boundary $\partial\Gamma_{12}$ belongs to the interior of a face of an element of $\mathcal{T}_{h,2}$. We consider two possibilities for the flow discretization on Ω_1 .

The first choice, which follows [24], is to let $\mathbf{X}_{h,1} \times M_{h,1}$ be any of the known conforming and stable Stokes finite element spaces, for example, the MINI elements [3], the Taylor–Hood elements [32], or the conforming Crouzeix–Raviart elements [17].

We assume that $\mathbf{X}_{h,1}$ and $M_{h,1}$ include at least polynomials of degree k_1 and $k_1 - 1$, respectively ($k_1 \geq 1$).

The second choice, following [28], is to let $\mathbf{X}_{h,1} \times M_{h,1}$ be a pair of discontinuous piecewise polynomial spaces such that on each element of $\mathcal{T}_{h,1}$ the space $\mathbf{X}_{h,1}$ contains vectors with component polynomials of degree k_1 and the space $M_{h,1}$ contains polynomials of degree $k_1 - 1$. In this second case, we assume that $\Omega \subset \mathbb{R}^2$.

In both cases, for the discretization of the Darcy model in Ω_2 , we take $\mathbf{X}_{h,2} \times M_{h,2}$ to be any of the standard MFE spaces, the Raviart–Thomas–Nedelec (RTN) spaces [27, 26], the Brezzi–Douglas–Marini (BDM) spaces [8], the Brezzi–Douglas–Fortin–Marini (BDFM) spaces [7], the Brezzi–Douglas–Duràn–Fortin (BDDF) spaces [6], or the Chen–Douglas (CD) spaces [11]. We assume that $\mathbf{X}^{h,1}$ and $M^{h,2}$ contain at least polynomials of degree k_2 and l_2 , respectively.

The analysis in both [24] and [28] allows for nonmatching grids across Γ_{12} , even though this is not explicitly stated in [24].

Let

$$\mathbf{X}_h = \mathbf{X}_{h,1} \times \mathbf{X}_{h,2}, \quad M_h = \{w = (w_1, w_2) \in M_{h,1} \times M_{h,2} : (w_1, 1)_{\Omega_1} + (w_2, 1)_{\Omega_2} = 0\}$$

and

$$\mathbf{X}_{h,0} = \{\mathbf{v} = (\mathbf{v}_1, \mathbf{v}_2) \in \mathbf{X}_h : \langle \mathbf{v}_1 \cdot \mathbf{n}_1 + \mathbf{v}_2 \cdot \mathbf{n}_2, \mu \rangle_{\Gamma_{12}} = 0 \quad \forall \mu \in \mathbf{X}_{h,2} \cdot \mathbf{n}_2\}.$$

To save space we will present only the method based on conforming Stokes elements [24]. We refer the reader to [28] for details on the discontinuous Stokes discretization for the coupled Stokes–Darcy problem. Let

$$\mathbf{X}_{h,1}^0 = \{\mathbf{v} \in \mathbf{X}_{h,1} : \mathbf{v} = 0 \text{ on } \Gamma_1\},$$

$$\mathbf{X}_{h,2}^0 = \{\mathbf{v} \in \mathbf{X}_{h,2} : \mathbf{v} \cdot \mathbf{n} = 0 \text{ on } \Gamma_2\},$$

$$\mathbf{X}_h^0 = \mathbf{X}_{h,1}^0 \times \mathbf{X}_{h,2}^0, \quad \text{and} \quad \mathbf{X}_{h,0}^0 = \mathbf{X}_h^0 \cap \mathbf{X}_{h,0}.$$

Let $\mathbf{u}_g \in H(\text{div}; \Omega)$ be such that $\mathbf{u}_g|_{\Omega_1} \in H^1(\Omega_1)$, $\mathbf{u}_g = \mathbf{g}_1$ on Γ_1 , and $\mathbf{u}_g \cdot \mathbf{n}_2 = g_2$ on Γ_2 . Let $\mathbf{U}_g \in \mathbf{X}_{h,0}$ be a suitable approximation to \mathbf{u}_g . The numerical scheme for the coupled Stokes–Darcy flow problem is as follows: find $\mathbf{U} \in \mathbf{X}_{h,0}^0 + \mathbf{U}_g$ and $P \in M_h$ such that

$$(3.1) \quad a(\mathbf{U}, \mathbf{v}) + b(\mathbf{v}, P) = (\mathbf{f}, \mathbf{v}) \quad \forall \mathbf{v} \in \mathbf{X}_{h,0}^0,$$

$$(3.2) \quad b(\mathbf{U}, w) = -(q_2, w)_{\Omega_2} \quad \forall w \in M_h,$$

where $a(\cdot, \cdot) = a_1(\cdot, \cdot) + a_2(\cdot, \cdot)$, $b(\cdot, \cdot) = b_1(\cdot, \cdot) + b_2(\cdot, \cdot)$,

$$a_1(\mathbf{u}_1, \mathbf{v}_1) = (2\mu \mathbf{D}(\mathbf{u}_1), \mathbf{D}(\mathbf{v}_1))_{\Omega_1} + \sum_{j=1}^{d-1} \left\langle \frac{\mu \alpha}{\sqrt{K_j}} \mathbf{u}_1 \cdot \boldsymbol{\tau}_j, \mathbf{v}_1 \cdot \boldsymbol{\tau}_j \right\rangle_{\Gamma_{12}},$$

$$a_2(\mathbf{u}_2, \mathbf{v}_2) = (\mu \mathbf{K}^{-1} \mathbf{u}_2, \mathbf{v}_2)_{\Omega_2}, \quad \text{and} \quad b_i(\mathbf{v}_i, w_i) = -(\nabla \cdot \mathbf{v}_i, w_i)_{\Omega_i}, \quad i = 1, 2.$$

We take \mathbf{U}_g to be any function in $\mathbf{X}_{h,0}$ such that $\mathbf{U}_g = Q_{h,1} \mathbf{g}_1$ on Γ_1 and $\mathbf{U}_g \cdot \mathbf{n}_2 = Q_{h,2} g_2$ on Γ_2 , where $Q_{h,1}$ is the $L^2(\Gamma_1)$ -projection onto $\mathbf{X}_{h,1}|_{\Gamma_1}$ and $Q_{h,2}$ is the $L^2(\Gamma_2)$ -projection onto $\mathbf{X}_{h,2} \cdot \mathbf{n}_2|_{\Gamma_2}$. The computed flow solution is independent of the choice

of \mathbf{U}_g and depends only on $Q_{h,1}\mathbf{g}_1$ and $Q_{h,2}g_2$. For the homogeneous boundary conditions case, it was shown in [24] that the above method has a unique solution satisfying

$$(3.3) \quad \|\mathbf{u} - \mathbf{U}\|_X + \|p - P\|_M \leq K(h_1^{k_1} + h_2^{k_2+1} + h_2^{l_2+1}),$$

assuming \mathbf{u} and p are smooth enough, where

$$\|\mathbf{v}\|_X^2 = \|\mathbf{v}_1\|_{H^1(\Omega_1)}^2 + \|\mathbf{v}_2\|_{L^2(\Omega_2)}^2 + \|\nabla \cdot \mathbf{v}_2\|_{L^2(\Omega_2)}^2, \quad \|w\|_M = \|w\|_{L^2(\Omega)}.$$

The results easily extend to the nonhomogeneous case considered here.

We show later that the error in the transport equations depends on the error in the approximation of the velocity on Γ . The approximation properties of $Q_{h,1}$ and $Q_{h,2}$ imply that

$$(3.4) \quad \|(\mathbf{u} - \mathbf{U}) \cdot \mathbf{n}\|_\Gamma \leq K(h_1^{k_1+1} + h_2^{k_2+1}).$$

Usually no flow boundary conditions $\mathbf{u}_2 \cdot \mathbf{n}_2 = 0$ are specified on Γ_2 , corresponding to an impermeable rock surrounding the aquifer. In that case the second term on the right in the above bound vanishes.

4. Formulation of the LDG method for transport. We rewrite the transport equation in a mixed form by introducing the diffusive flux

$$(4.1) \quad \mathbf{z} = -\mathbf{D}\nabla c.$$

The system (2.11)–(2.14) is equivalent to

$$(4.2) \quad \phi c_t + \nabla \cdot (c\mathbf{u} + \mathbf{z}) = \phi s,$$

$$(4.3) \quad (c\mathbf{u} + \mathbf{z}) \cdot \mathbf{n} = c_{in} \mathbf{u} \cdot \mathbf{n} \quad \text{on } \Gamma_{in},$$

$$(4.4) \quad \mathbf{z} \cdot \mathbf{n} = 0 \quad \text{on } \Gamma_{out}.$$

Let \mathcal{T}_h be a shape-regular finite element partition of Ω . We denote by h_E the diameter of an element E and set h to be the maximum element diameter. We assume that no element E overlaps with both Γ_{in} and Γ_{out} and that each element E has a Lipschitz boundary ∂E . The partition \mathcal{T}_h may be different from $\mathcal{T}_{h,1}$ and $\mathcal{T}_{h,2}$. Let $W_E = H^1(E)$, $\mathbf{V}_E = (W_E)^d$, and let \mathbf{n}_E be the outward unit normal on ∂E . We will need some notation for values of discontinuous functions on element edges (faces in three dimensions). Let

$$W = \{w \in L^2(\Omega) : w \in W_E \forall E \in \mathcal{T}_h\}$$

$$V = \{v \in (L^2(\Omega))^d : v \in V_E \forall E \in \mathcal{T}_h\}$$

Let $w \in W$. For any $E \in \mathcal{T}_h$ and any $\mathbf{x} \in \partial E$ we define

$$(4.5) \quad w^-(\mathbf{x}) = \lim_{s \rightarrow 0^-} w(\mathbf{x} + s\mathbf{n}_E), \quad w^+(\mathbf{x}) = \lim_{s \rightarrow 0^+} w(\mathbf{x} + s\mathbf{n}_E),$$

$$(4.6) \quad \bar{w}(\mathbf{x}) = \frac{1}{2} (w^+(\mathbf{x}) + w^-(\mathbf{x})), \quad \text{and} \quad w^u(\mathbf{x}) = \begin{cases} w^-(\mathbf{x}) & \text{if } \mathbf{U} \cdot \mathbf{n}_E \geq 0 \\ w^+(\mathbf{x}) & \text{if } \mathbf{U} \cdot \mathbf{n}_E < 0. \end{cases}$$

For a vector function $\mathbf{v} \in \mathbf{V}$, \mathbf{v}^- , \mathbf{v}^+ , and $\bar{\mathbf{v}}$ are defined in a similar way. Note that the upwinding is based on the computed velocity U .

Assuming that the solution to (4.2)–(4.4) is smooth enough, multiplying by appropriate test functions on every element E and integrating by parts, we obtain the following weak formulation. For every $E \in \mathcal{T}_h$, $c \in W_E$ and $\mathbf{z} \in \mathbf{V}_E$ satisfy

$$(4.7) \quad (\mathbf{D}^{-1}\mathbf{z}, \mathbf{v})_E - (c, \nabla \cdot \mathbf{v})_E + \langle c, \mathbf{v}^- \cdot \mathbf{n}_E \rangle_{\partial E} = 0 \quad \forall \mathbf{v} \in \mathbf{V}_E,$$

$$(4.8) \quad \begin{aligned} &(\phi c_t, w)_E - (\mathbf{c}\mathbf{u} + \mathbf{z}, \nabla w)_E + \langle (\mathbf{c}\mathbf{u} + \mathbf{z}) \cdot \mathbf{n}_E, w^- \rangle_{\partial E \setminus \Gamma} + \langle \mathbf{c}\mathbf{u} \cdot \mathbf{n}_E, w^- \rangle_{\partial E \cap \Gamma_{out}} \\ &= (\phi s, w)_E - \langle c_{in} \mathbf{u} \cdot \mathbf{n}_E, w^- \rangle_{\partial E \cap \Gamma_{in}} \quad \forall w \in W_E. \end{aligned}$$

Let $W_{h,E} \subset W_E$ denote the space of all polynomials on E of degree $\leq k_E$, $k_E \geq 1$, and let $\mathbf{V}_{h,E} = (W_{h,E})^d$. Let $k = \min_E k_E$. On each element E , $c(\cdot, t)$ and $\mathbf{z}(\cdot, t)$ are approximated by $C(\cdot, t) \in W_{h,E}$ and $\mathbf{Z}(\cdot, t) \in \mathbf{V}_{h,E}$ respectively. Let

$$W_h := \{w \in L^2(\Omega) : w \in W_{h,E} \forall E \in \mathcal{T}_h\},$$

$$\mathbf{V}_h := \{\mathbf{v} \in (L^2(\Omega))^d : \mathbf{v} \in \mathbf{V}_{h,E}, \forall E \in \mathcal{T}_h\}.$$

Let $C^0 \in W_h$ be the L^2 -projection of c^0 :

$$(4.9) \quad \forall E \in \mathcal{T}_h, \quad (C^0 - c^0, w)_E = 0 \quad \forall w \in W_{h,E}.$$

The semidiscrete LDG method is defined as follows: for each $t \in [0, T]$ find $C(\cdot, t) \in W_h$ and $\mathbf{Z}(\cdot, t) \in \mathbf{V}_h$ such that on each $E \in \mathcal{T}_h$,

$$(4.10) \quad \begin{aligned} &(\mathbf{D}^{-1}\mathbf{Z}, \mathbf{v})_E - (C, \nabla \cdot \mathbf{v})_E + \langle \bar{C}, \mathbf{v}^- \cdot \mathbf{n}_E \rangle_{\partial E \setminus \Gamma} \\ &+ \langle C^-, \mathbf{v}^- \cdot \mathbf{n}_E \rangle_{\partial E \cap \Gamma} = 0 \quad \forall \mathbf{v} \in \mathbf{V}_{h,E}, \quad t \in [0, T], \end{aligned}$$

$$(4.11) \quad \begin{aligned} &(\phi C_t, w)_E - (C\mathbf{U} + \mathbf{Z}, \nabla w)_E + \langle (C^u \mathbf{U} + \bar{\mathbf{Z}}) \cdot \mathbf{n}_E, w^- \rangle_{\partial E \setminus \Gamma} \\ &+ \langle C^- \mathbf{U} \cdot \mathbf{n}_E, w^- \rangle_{\partial E \cap \Gamma_{out}} + \frac{1}{2} (C \nabla \cdot (\mathbf{u} - \mathbf{U}), w)_E \\ &+ \frac{1}{2} \langle C^- (\mathbf{u} - \mathbf{U}) \cdot \mathbf{n}_E, w^- \rangle_{\partial E \cap \Gamma_{out}} - \frac{1}{2} \langle C^- (\mathbf{u} - \mathbf{U}) \cdot \mathbf{n}_E, w^- \rangle_{\partial E \cap \Gamma_{in}} \\ &= (\phi s, w)_E - \langle c_{in} \mathbf{u} \cdot \mathbf{n}_E, w^- \rangle_{\partial E \cap \Gamma_{in}} \quad \forall w \in W_{h,E}, \quad t \in (0, T), \end{aligned}$$

$$(4.12) \quad C(\cdot, 0) = C^0.$$

The method is based on the weak formulation (4.7)–(4.8) with several modifications. The terms $\frac{1}{2}(C \nabla \cdot (\mathbf{u} - \mathbf{U}), w)_E$, $\frac{1}{2} \langle C^- (\mathbf{u} - \mathbf{U}) \cdot \mathbf{n}_E, w^- \rangle_{\partial E \cap \Gamma_{out}}$, and $-\frac{1}{2} \langle C^- (\mathbf{u} - \mathbf{U}) \cdot \mathbf{n}_E, w^- \rangle_{\partial E \cap \Gamma_{in}}$ have been added to the mass conservation equation. A term similar to the first one, but with a different scaling, has been used in [20]. These terms can be viewed as corrections for the error in approximating $\nabla \cdot \mathbf{u}$ and $\mathbf{u} \cdot \mathbf{n}$ on Γ . As we show later, they provide better stability properties of the method without affecting the accuracy. Note also that the true normal velocity $\mathbf{u} \cdot \mathbf{n}$ is used on the right-hand side in the Γ_{in} -term. Furthermore, the average concentration value is used on the

interior edges (faces) in the diffusive flux equation, while upwinding is used in the conservation equation.

In the above scheme we assume that high enough quadrature rules are used so that the numerical integration error is dominated by the discretization error. Note that the computed velocity \mathbf{U} is needed to evaluate element and edge integrals in (4.11). As a result \mathbf{U} needs to be evaluated at any quadrature point in E or on ∂E . Since we allow for the flow and transport grids to differ and the velocity approximation could be discontinuous, \mathbf{U} may not be well defined at a given quadrature point. This problem is handled by decomposing E into subelements according to its intersection with the flow grid. More precisely, let $E_i^{X_h}$, $i = 1, \dots, m_E$ be the elements of the flow grid that overlap with E . Then we have

$$\int_E \varphi \, d\mathbf{x} = \sum_{i=1}^{m_E} \int_{E \cap E_i^{X_h}} \varphi \, d\mathbf{x}, \quad \int_{\partial E} \varphi \, d\sigma = \sum_{i=1}^{m_E} \int_{\partial E \cap E_i^{X_h}} \varphi \, d\sigma.$$

The computed velocity \mathbf{U} is well defined on all subelements and subedges.

In this paper we restrict our attention to the semidiscrete formulation. Standard methods such as Euler or Runge–Kutta can be employed for the time discretization; see, e.g., [16].

5. Stability of the LDG scheme. The stability argument is based on the analysis in [13]. The main difference here is that we allow for velocity with nonzero divergence as well as account for the use of an approximate velocity in the transport equation.

By adding (4.10) and (4.11), summing over all the elements, and integrating over t , we obtain the equivalent formulation

$$(5.1) \quad B_{\mathbf{U}}(C, \mathbf{Z}; w, \mathbf{v}) = - \int_0^T \langle c_{in} \mathbf{u} \cdot \mathbf{n}, w^- \rangle_{\Gamma_{in}} \, dt + \int_0^T (\phi_s, w) \, dt$$

$$\forall (w, \mathbf{v}) \in C^0(0, T; W_h \times \mathbf{V}_h),$$

where

$$(5.2) \quad B_{\mathbf{U}}(C, \mathbf{Z}; w, \mathbf{v}) := \int_0^T \sum_E \left\{ (\phi C_t, w)_E - (C\mathbf{U} + \mathbf{Z}, \nabla w)_E \right.$$

$$+ \langle C^- \mathbf{U} \cdot \mathbf{n}_E, w^- \rangle_{\partial E \cap \Gamma_{out}} + \langle (C^u \mathbf{U} + \bar{\mathbf{Z}}) \cdot \mathbf{n}_E, w^- \rangle_{\partial E \setminus \Gamma} + (\mathbf{D}^{-1} \mathbf{Z}, \mathbf{v})_E$$

$$- (C, \nabla \cdot \mathbf{v})_E + \langle \bar{C}, \mathbf{v}^- \cdot \mathbf{n}_E \rangle_{\partial E \setminus \Gamma} + \langle C^-, \mathbf{v}^- \cdot \mathbf{n}_E \rangle_{\partial E \cap \Gamma}$$

$$+ \frac{1}{2} (\nabla \cdot (\mathbf{u} - \mathbf{U}) C, w)_E + \frac{1}{2} \langle C^- (\mathbf{u} - \mathbf{U}) \cdot \mathbf{n}_E, w^- \rangle_{\partial E \cap \Gamma_{out}}$$

$$\left. - \frac{1}{2} \langle C^- (\mathbf{u} - \mathbf{U}) \cdot \mathbf{n}_E, w^- \rangle_{\partial E \cap \Gamma_{in}} \right\} dt.$$

Taking $w = C$ and $\mathbf{v} = \mathbf{Z}$, we have

$$(5.3) \quad B_{\mathbf{U}}(C, \mathbf{Z}; C, \mathbf{Z}) = \Theta_1 + \Theta_2 + \Theta_3,$$

where

$$\begin{aligned}
 (5.4) \quad \Theta_1 &= \int_0^T \sum_E \{(\phi C_t, C)_E + (\mathbf{D}^{-1}\mathbf{Z}, \mathbf{Z})_E\} dt, \\
 \Theta_2 &= \int_0^T \sum_E \left\{ - (C\mathbf{U}, \nabla C)_E + \langle C^u \mathbf{U} \cdot \mathbf{n}_E, C^- \rangle_{\partial E \setminus \Gamma} + \langle C^- \mathbf{U} \cdot \mathbf{n}_E, C^- \rangle_{\partial E \cap \Gamma_{out}} \right. \\
 &\quad \left. + \frac{1}{2} (C \nabla \cdot (\mathbf{u} - \mathbf{U}), C)_E + \frac{1}{2} \langle C^- (\mathbf{u} - \mathbf{U}) \cdot \mathbf{n}_E, C^- \rangle_{\partial E \cap \Gamma_{out}} \right. \\
 &\quad \left. - \frac{1}{2} \langle C^- (\mathbf{u} - \mathbf{U}) \cdot \mathbf{n}_E, w^- \rangle_{\partial E \cap \Gamma_{in}} \right\} dt, \\
 \Theta_3 &= \int_0^T \sum_E \left\{ - (\mathbf{Z}, \nabla C)_E + \langle \bar{\mathbf{Z}} \cdot \mathbf{n}_E, C^- \rangle_{\partial E \setminus \Gamma} - (C, \nabla \cdot \mathbf{Z})_E \right. \\
 &\quad \left. + \langle \bar{C}, \mathbf{Z}^- \cdot \mathbf{n}_E \rangle_{\partial E \setminus \Gamma} + \langle C^-, \mathbf{Z}^- \cdot \mathbf{n}_E \rangle_{\partial E \cap \Gamma} \right\} dt.
 \end{aligned}$$

Since

$$(\phi C_t, C)_E = \frac{1}{2} \frac{d}{dt} (\phi^{1/2} C, \phi^{1/2} C)_E,$$

we can write

$$(5.5) \quad \Theta_1 = \frac{1}{2} \|\phi^{1/2} C(T)\|^2 - \frac{1}{2} \|\phi^{1/2} C(0)\|^2 + \int_0^T \|\mathbf{D}^{-1/2} \mathbf{Z}\|^2 dt.$$

We continue with the bound on Θ_2 . Integration by parts gives

$$(C\mathbf{U}, \nabla C)_E = \frac{1}{2} \int_{\partial E} (C^-)^2 \mathbf{U} \cdot \mathbf{n}_E \, d\sigma - \frac{1}{2} \int_E C^2 \nabla \cdot \mathbf{U} \, dx.$$

Then we have

$$\begin{aligned}
 (5.6) \quad \Theta_2 &= \int_0^T \sum_E \left\{ -\frac{1}{2} \langle C^- \mathbf{U} \cdot \mathbf{n}_E, C^- \rangle_{\partial E \setminus \Gamma} - \frac{1}{2} \langle C^- \mathbf{u} \cdot \mathbf{n}_E, C^- \rangle_{\partial E \cap \Gamma_{in}} \right. \\
 &\quad \left. + \frac{1}{2} \langle C^- \mathbf{u} \cdot \mathbf{n}_E, C^- \rangle_{\partial E \cap \Gamma_{out}} + \frac{1}{2} (C^2, \nabla \cdot \mathbf{u})_E + \langle C^u \mathbf{U} \cdot \mathbf{n}_E, C^- \rangle_{\partial E \setminus \Gamma} \right\} dt \\
 &= \int_0^T \left\{ \frac{1}{2} (C^2, \nabla \cdot \mathbf{u}) + \frac{1}{2} \langle |\mathbf{u} \cdot \mathbf{n}|, (C^-)^2 \rangle_\Gamma \right. \\
 &\quad \left. + \sum_E \left\langle \left(C^u - \frac{1}{2} C^- \right) \mathbf{U} \cdot \mathbf{n}_E, C^- \right\rangle_{\partial E \setminus \Gamma} \right\} dt.
 \end{aligned}$$

It is convenient to express the sum over the elements in the last term in (5.6) as a sum over the interior element edges (faces) $\{e\}$. Let $e \in \partial E$ be an interior edge (face) of the element E . For $w \in W_h$ and $\mathbf{v} \in \mathbf{V}_h$, we set on e ,

$$[w] = (w^- - w^+) \mathbf{n}_E, \quad [\mathbf{v}] = (\mathbf{v}^- - \mathbf{v}^+) \cdot \mathbf{n}_E.$$

Note that these definitions do not depend on which element E is taken as a reference. Let us also fix arbitrarily a unit normal vector on e , denoted by \mathbf{n}_e . Since

$$\frac{1}{2}[C^2] = \frac{1}{2}((C^-)^2 - (C^+)^2)\mathbf{n}_E = \frac{1}{2}(C^- + C^+)(C^- - C^+)\mathbf{n}_E = \bar{C}[C],$$

we can write

$$\begin{aligned} \sum_E \left\langle \left(C^u - \frac{1}{2}C^- \right) \mathbf{U} \cdot \mathbf{n}_E, C^- \right\rangle_{\partial E \setminus \Gamma} &= \sum_e \left\langle \mathbf{U} \cdot \left(C^u[C] - \frac{1}{2}[C^2] \right), 1 \right\rangle_e \\ &= \sum_e \langle \mathbf{U} \cdot (C^u[C] - \bar{C}[C]), 1 \rangle_e \\ (5.7) \qquad \qquad \qquad &= \sum_e \langle \mathbf{U} \cdot [C](C^u - \bar{C}), 1 \rangle_e \\ &= \frac{1}{2} \sum_e \langle |\mathbf{U} \cdot \mathbf{n}_e|, [C] \cdot [C] \rangle_e, \end{aligned}$$

where we used in the last equality that on any $e \in \partial E$,

$$\begin{aligned} \mathbf{U} \cdot [C](C^u - \bar{C}) &= \mathbf{U} \cdot \mathbf{n}_E(C^- - C^+) \left(\left\{ \begin{array}{l} C^-, \mathbf{U} \cdot \mathbf{n}_E \geq 0 \\ C^+, \mathbf{U} \cdot \mathbf{n}_E < 0 \end{array} \right\} - \frac{C^- + C^+}{2} \right) \\ &= \mathbf{U} \cdot \mathbf{n}_E(C^- - C^+) \frac{(C^- - C^+)}{2} \text{sign}(\mathbf{U} \cdot \mathbf{n}_E) = \frac{1}{2} |\mathbf{U} \cdot \mathbf{n}_E| [C] \cdot [C]. \end{aligned}$$

Substituting (5.7) into (5.6) we obtain

$$(5.8) \quad \Theta_2 = \frac{1}{2} \int_0^T \left\{ (C^2, \nabla \cdot \mathbf{u}) + \langle |\mathbf{u} \cdot \mathbf{n}|, (C^-)^2 \rangle_\Gamma + \sum_e \langle |\mathbf{U} \cdot \mathbf{n}_e|, [C] \cdot [C] \rangle_e \right\} dt.$$

To estimate Θ_3 we use Green’s formula to obtain

$$\begin{aligned} \Theta_3 &= \int_0^T \sum_E \left\{ -\langle \mathbf{Z}^- \cdot \mathbf{n}_E, C^- \rangle_{\partial E \setminus \Gamma} + \frac{1}{2} \langle (\mathbf{Z}^+ + \mathbf{Z}^-) \cdot \mathbf{n}_E, C^- \rangle_{\partial E \setminus \Gamma} \right. \\ (5.9) \qquad \qquad \qquad &\qquad \qquad \left. + \frac{1}{2} \langle C^+ + C^-, \mathbf{Z}^- \cdot \mathbf{n}_E \rangle_{\partial E \setminus \Gamma} \right\} dt \\ &= \int_0^T \sum_E \left\{ \frac{1}{2} \langle C^+, \mathbf{Z}^- \cdot \mathbf{n}_E \rangle_{\partial E \setminus \Gamma} + \frac{1}{2} \langle \mathbf{Z}^+ \cdot \mathbf{n}_E, C^- \rangle_{\partial E \setminus \Gamma} \right\} dt = 0, \end{aligned}$$

where the last equality follows from the fact that on each interior edge (face) the contributions from the two adjacent elements cancel, due to the opposite directions of the outward normal vectors. A combination of (5.3), (5.5), (5.8), and (5.9) gives

$$\begin{aligned} B_{\mathbf{U}}(C, \mathbf{Z}; C, \mathbf{Z}) &= \frac{1}{2} \|\phi^{1/2} C(T)\|^2 - \frac{1}{2} \|\phi^{1/2} C(0)\|^2 + \int_0^T \|\mathbf{D}^{-1/2} \mathbf{Z}\|^2 dt \\ (5.10) \qquad \qquad \qquad &+ \frac{1}{2} \int_0^T \left\{ (C^2, \nabla \cdot \mathbf{u}) + \langle |\mathbf{u} \cdot \mathbf{n}|, (C^-)^2 \rangle_\Gamma + \sum_e \langle |\mathbf{U} \cdot \mathbf{n}_e|, [C] \cdot [C] \rangle_e \right\} dt. \end{aligned}$$

Combining (5.1) and (5.10) and using Young’s inequality

$$(5.11) \qquad \qquad \qquad ab \leq \frac{\epsilon}{2} a^2 + \frac{1}{2\epsilon} b^2 \quad , \quad a, b \in \mathbb{R} \quad , \quad \epsilon > 0,$$

with $\epsilon = 1$, we obtain

$$\begin{aligned}
 (5.12) \quad & \frac{1}{2} \|\phi^{1/2} C(T)\|^2 + \int_0^T \|\mathbf{D}^{-1/2} \mathbf{Z}\|^2 dt \\
 & \leq \frac{1}{2} \|\phi^{1/2} C(0)\|^2 + \frac{1}{2} \int_0^T (C^2, (\nabla \cdot \mathbf{u})_-) dt \\
 & \quad + \frac{1}{2} \int_0^T \langle |\mathbf{u} \cdot \mathbf{n}|, (c_{in})^2 \rangle_{\Gamma_{in}} dt + \int_0^T \|\phi^{1/2} s\| \|\phi^{1/2} C\| dt,
 \end{aligned}$$

where

$$(\nabla \cdot \mathbf{u})_- := \begin{cases} 0, & \nabla \cdot \mathbf{u} \geq 0, \\ -\nabla \cdot \mathbf{u}, & \nabla \cdot \mathbf{u} < 0. \end{cases}$$

For the second term on the right in (5.12) we have

$$\frac{1}{2} \int_0^T (C^2, (\nabla \cdot \mathbf{u})_-) dt \leq \frac{1}{2} \|\phi^{-1} (\nabla \cdot \mathbf{u})_-\|_{0,\infty} \int_0^T \|\phi^{1/2} C(t)\|^2 dt,$$

and the use of Gronwall’s inequality implies

$$\begin{aligned}
 (5.13) \quad & \|\phi^{1/2} C(T)\|^2 + 2 \int_0^T \|\mathbf{D}^{-1/2} \mathbf{Z}\|^2 dt \\
 & \leq e^{LT} \left(\|\phi^{1/2} C(0)\|^2 + \int_0^T \langle |\mathbf{u} \cdot \mathbf{n}|, (c_{in})^2 \rangle_{\Gamma_{in}} dt + 2 \int_0^T \|\phi^{1/2} s\| \|\phi^{1/2} C\| dt \right),
 \end{aligned}$$

where $L := \|\phi^{-1} (\nabla \cdot \mathbf{u})_-\|_{0,\infty}$. Using (4.9),

$$(5.14) \quad \|\phi^{1/2} C(0)\| \leq (\phi^*)^{1/2} \|c^0\|.$$

To complete the stability analysis we need the following result shown in [13].

LEMMA 5.1. *Suppose that for all $T > 0$,*

$$\chi^2(T) + R(T) \leq A(T) + 2 \int_0^T B(t) \chi(t) dt,$$

where R, A , and B are nonnegative functions. Then

$$\sqrt{\chi^2 + R(T)} \leq \sup_{0 \leq t \leq T} A^{1/2}(t) + \int_0^T B(t) dt.$$

Let us define the norm $\| \! \| (C, \mathbf{Z}) \! \|$ by

$$(5.15) \quad \| \! \| (C, \mathbf{Z}) \! \| \|^2 := \|\phi^{1/2} C(T)\|^2 + 2 \int_0^T \|\mathbf{D}^{-1/2} \mathbf{Z}\|^2 dt.$$

Then, using (5.13), (5.14), and Lemma 5.1, we obtain the following stability result.

THEOREM 5.2. *The solution to the semidiscrete LDG method (4.10)–(4.12) satisfies*

$$(5.16) \quad \| \! \| (C, \mathbf{Z}) \! \| \leq e^{LT/2} \left(\phi^* \|c^0\|^2 + \int_0^T \langle |\mathbf{u} \cdot \mathbf{n}|, (c_{in})^2 \rangle_{\Gamma_{in}} dt \right)^{1/2} + e^{LT} \int_0^T \|\phi^{1/2} s\| dt,$$

where L is defined in (5.13).

Remark 5.1. Note that, due to including the additional terms in the scheme, the stability estimate depends on the true velocity, $\nabla \cdot \mathbf{u}$ and $\mathbf{u} \cdot \mathbf{n}$ on Γ_{in} , rather than on the computed velocity \mathbf{U} .

6. Error analysis of the LDG scheme. Let $\Pi c \in W_h$, $\Pi \mathbf{z} \in \mathbf{V}_h$, and $\Pi \mathbf{u} \in \mathbf{V}_h$ denote the L^2 -projections of c , \mathbf{z} , and \mathbf{u} , respectively:

$$(6.1) \quad \forall E \in \mathcal{T}_h, \quad (c - \Pi c, w)_E = 0 \quad \forall w \in W_{h,E},$$

$$(6.2) \quad \forall E \in \mathcal{T}_h, \quad (\mathbf{z} - \Pi \mathbf{z}, \mathbf{v})_E = 0 \quad \forall \mathbf{v} \in \mathbf{V}_{h,E},$$

$$(6.3) \quad \forall E \in \mathcal{T}_h, \quad (\mathbf{u} - \Pi \mathbf{u}, \mathbf{v})_E = 0 \quad \forall \mathbf{v} \in \mathbf{V}_{h,E}.$$

The L^2 -projection has the approximation property [12]

$$(6.4) \quad \|q - \Pi q\|_{m,p,E} \leq K h_E^{l-m} \|q\|_{l,p,E}, \quad 0 \leq m \leq l \leq k_E + 1, \quad 1 \leq p \leq \infty,$$

where q is either a scalar or a vector function. We will also make use of the trace inequality [4]

$$(6.5) \quad \forall e \in \partial E, \quad \|\chi\|_e \leq K \left(h_E^{-1/2} \|\chi\|_E + h_E^{1/2} |\chi|_{1,E} \right) \quad \forall \chi \in H^1(E).$$

Using (6.4) and (6.5),

$$(6.6) \quad \|q - \Pi q\|_e \leq K h_E^{l-1/2} \|q\|_{l,E}, \quad 1 \leq l \leq k_E + 1.$$

For polynomial functions, (6.5) and the inverse inequality [12]

$$(6.7) \quad \|w\|_{1,E} \leq K h_E^{-1} \|w\|_E$$

imply

$$(6.8) \quad \|w\|_e \leq K h_E^{-1/2} \|w\|_E.$$

Similarly to the discrete variational formulation (5.1), the weak solution of (4.7)–(4.8) satisfies

$$(6.9) \quad B_{\mathbf{u}}(c, \mathbf{z}; w, \mathbf{v}) = - \int_0^T \langle c_{in} \mathbf{u} \cdot \mathbf{n}, w^- \rangle_{\Gamma_{in}} dt + \int_0^T (\phi s, w) dt$$

$$\forall (w, \mathbf{v}) \in C^0(0, T; W \times \mathbf{V}),$$

where

$$(6.10) \quad B_{\mathbf{u}}(c, \mathbf{z}; w, \mathbf{v}) := \int_0^T \sum_E \left\{ (\phi c_t, w)_E - (c \mathbf{u} + \mathbf{z}, \nabla w)_E \right.$$

$$\left. + \langle c^- \mathbf{u} \cdot \mathbf{n}_E, w^- \rangle_{\partial E \cap \Gamma_{out}} + \langle (c^u \mathbf{u} + \bar{\mathbf{z}}) \cdot \mathbf{n}_E, w^- \rangle_{\partial E \setminus \Gamma} + (\mathbf{D}^{-1} \mathbf{z}, \mathbf{v})_E \right.$$

$$\left. - (c, \nabla \cdot \mathbf{v})_E + \langle \bar{c}, \mathbf{v}^- \cdot \mathbf{n}_E \rangle_{\partial E \setminus \Gamma} + \langle c^-, \mathbf{v}^- \cdot \mathbf{n}_E \rangle_{\partial E \cap \Gamma} \right\} dt.$$

Subtracting (5.1) from (6.9) gives

$$(6.11) \quad B_{\mathbf{u}}(c, \mathbf{z}; w, \mathbf{v}) - B_{\mathbf{U}}(C, \mathbf{Z}; w, \mathbf{v}) = 0.$$

Let $\psi_c = C - \Pi c$, $\psi_{\mathbf{z}} = \mathbf{Z} - \Pi \mathbf{z}$, $\theta_c = c - \Pi c$, and $\theta_{\mathbf{z}} = \mathbf{z} - \Pi \mathbf{z}$. Setting $(w, \mathbf{v}) = (\psi_c, \psi_{\mathbf{z}})$ in (6.11), we get

(6.12)

$$B_{\mathbf{U}}(\psi_c, \psi_{\mathbf{z}}; \psi_c, \psi_{\mathbf{z}}) = B_{\mathbf{u}}(\theta_c, \theta_{\mathbf{z}}; \psi_c, \psi_{\mathbf{z}}) + B_{\mathbf{u}}(\Pi c, \Pi \mathbf{z}; \psi_c, \psi_{\mathbf{z}}) - B_{\mathbf{U}}(\Pi c, \Pi \mathbf{z}; \psi_c, \psi_{\mathbf{z}}).$$

For the error due to the velocity approximation, we have

(6.13)

$$\begin{aligned} & B_{\mathbf{u}}(\Pi c, \Pi \mathbf{z}; \psi_c, \psi_{\mathbf{z}}) - B_{\mathbf{U}}(\Pi c, \Pi \mathbf{z}; \psi_c, \psi_{\mathbf{z}}) \\ &= \int_0^T \sum_E \left\{ -(\Pi c(\mathbf{u} - \mathbf{U}), \nabla \psi_c)_E + \langle (\Pi c)^u (\mathbf{u} - \mathbf{U}) \cdot \mathbf{n}_E, \psi_c^- \rangle_{\partial E \setminus \Gamma} \right. \\ &\quad + \langle (\Pi c)^- (\mathbf{u} - \mathbf{U}) \cdot \mathbf{n}_E, \psi_c^- \rangle_{\partial E \cap \Gamma_{out}} - \frac{1}{2}(\Pi c \nabla \cdot (\mathbf{u} - \mathbf{U}), \psi_c)_E \\ &\quad \left. - \frac{1}{2} \langle (\Pi c)^- (\mathbf{u} - \mathbf{U}) \cdot \mathbf{n}_E, \psi_c^- \rangle_{\partial E \cap \Gamma_{out}} + \frac{1}{2} \langle (\Pi c)^- (\mathbf{u} - \mathbf{U}) \cdot \mathbf{n}_E, \psi_c^- \rangle_{\partial E \cap \Gamma_{in}} \right\} dt \\ &= \int_0^T \sum_E \left\{ (\nabla \cdot (\Pi c(\mathbf{u} - \mathbf{U})), \psi_c)_E + \langle ((\Pi c)^u - (\Pi c)^-)(\mathbf{u} - \mathbf{U}) \cdot \mathbf{n}_E, \psi_c^- \rangle_{\partial E \setminus \Gamma} \right. \\ &\quad \left. - \frac{1}{2}(\Pi c \nabla \cdot (\mathbf{u} - \mathbf{U}), \psi_c)_E - \frac{1}{2} \langle (\Pi c)^- (\mathbf{u} - \mathbf{U}) \cdot \mathbf{n}_E, \psi_c^- \rangle_{\partial E \cap \Gamma} \right\} dt. \end{aligned}$$

Substituting (6.13) into (6.12) and using the definition (6.10) for $B_{\mathbf{u}}(\theta_c, \theta_{\mathbf{z}}; \psi_c, \psi_{\mathbf{z}})$, we obtain

(6.14)

$$\begin{aligned} B_{\mathbf{U}}(\psi_c, \psi_{\mathbf{z}}; \psi_c, \psi_{\mathbf{z}}) &= \int_0^T \sum_E \left\{ (\phi(\theta_c)_t, \psi_c)_E - (\theta_c \mathbf{u}, \nabla \psi_c)_E - (\theta_{\mathbf{z}}, \nabla \psi_c)_E \right. \\ &\quad + \langle \theta_c^u \mathbf{u} \cdot \mathbf{n}_E, \psi_c^- \rangle_{\partial E \setminus \Gamma} + \langle \overline{\theta_{\mathbf{z}}} \cdot \mathbf{n}_E, \psi_c^- \rangle_{\partial E \setminus \Gamma} + \langle \theta_c^- \mathbf{u} \cdot \mathbf{n}_E, \psi_c^- \rangle_{\partial E \cap \Gamma_{out}} \\ &\quad + (\mathbf{D}^{-1} \theta_{\mathbf{z}}, \psi_{\mathbf{z}})_E - (\theta_c, \nabla \cdot \psi_{\mathbf{z}})_E + \langle \overline{\theta_c}, \psi_{\mathbf{z}}^- \cdot \mathbf{n}_E \rangle_{\partial E \setminus \Gamma} + \langle \theta_c^-, \psi_{\mathbf{z}}^- \cdot \mathbf{n}_E \rangle_{\partial E \cap \Gamma} \\ &\quad + (\nabla \cdot (\Pi c(\mathbf{u} - \mathbf{U})), \psi_c)_E + \langle ((\Pi c)^u - (\Pi c)^-)(\mathbf{u} - \mathbf{U}) \cdot \mathbf{n}_E, \psi_c^- \rangle_{\partial E \setminus \Gamma} \\ &\quad \left. - \frac{1}{2}(\Pi c \nabla \cdot (\mathbf{u} - \mathbf{U}), \psi_c)_E - \frac{1}{2} \langle (\Pi c)^- (\mathbf{u} - \mathbf{U}) \cdot \mathbf{n}_E, \psi_c^- \rangle_{\partial E \cap \Gamma} \right\} dt. \end{aligned}$$

We now rewrite the summation over the elements in (6.14) in terms of a summation over the interior edges (faces) where it is relevant:

(6.15)

$$\begin{aligned} B_{\mathbf{U}}(\psi_c, \psi_{\mathbf{z}}; \psi_c, \psi_{\mathbf{z}}) &= \int_0^T \sum_E \left\{ (\phi(\theta_c)_t, \psi_c)_E - (\theta_c \mathbf{u}, \nabla \psi_c)_E - (\theta_{\mathbf{z}}, \nabla \psi_c)_E \right. \\ &\quad + (\mathbf{D}^{-1} \theta_{\mathbf{z}}, \psi_{\mathbf{z}})_E - (\theta_c, \nabla \cdot \psi_{\mathbf{z}})_E + (\nabla \cdot (\Pi c(\mathbf{u} - \mathbf{U})), \psi_c)_E \\ &\quad \left. - \frac{1}{2}(\Pi c \nabla \cdot (\mathbf{u} - \mathbf{U}), \psi_c)_E + \langle ((\Pi c)^u - (\Pi c)^-)(\mathbf{u} - \mathbf{U}) \cdot \mathbf{n}_E, \psi_c^- \rangle_{\partial E \setminus \Gamma} \right\} dt \\ &\quad + \int_0^T \sum_e \left\{ \langle \theta_c^u \mathbf{u}, [\psi_c] \rangle_e + \langle \overline{\theta_{\mathbf{z}}}, [\psi_c] \rangle_e + \langle \overline{\theta_c}, [\psi_{\mathbf{z}}] \rangle_e \right\} dt \\ &\quad + \int_0^T \left\{ \langle \theta_c^- \mathbf{u} \cdot \mathbf{n}, \psi_c^- \rangle_{\Gamma_{out}} + \langle \theta_c^-, \psi_{\mathbf{z}}^- \cdot \mathbf{n} \rangle_{\Gamma} \right. \\ &\quad \left. - \frac{1}{2} \langle (\Pi c)^- (\mathbf{u} - \mathbf{U}) \cdot \mathbf{n}_E, \psi_c^- \rangle_{\Gamma} \right\} dt \equiv T_1 + T_2 + \dots + T_{14}. \end{aligned}$$

Using (5.10) and (4.9), (6.15) implies

$$(6.16) \quad \frac{1}{2} \|\phi^{1/2} \psi_c(T)\|^2 + \int_0^T \|\mathbf{D}^{-1/2} \psi_{\mathbf{z}}\|^2 dt \leq \frac{1}{2} \int_0^T (\psi_c^2, (\nabla \cdot \mathbf{u})_-) dt + T_1 + T_2 + \dots + T_{14}.$$

For the first term on the right above, we have

$$(6.17) \quad \frac{1}{2} \int_0^T (\psi_c^2, (\nabla \cdot \mathbf{u})_-) dt \leq \frac{1}{2} \|\phi^{-1} (\nabla \cdot \mathbf{u})_-\|_{0,\infty} \int_0^T \|\phi^{1/2} \psi_c(t)\|^2 dt.$$

We continue with bounds on the other terms on the right in (6.16).

From the definition of the L^2 -projections (6.1) and (6.2), it follows that

$$(6.18) \quad T_3 = T_5 = 0.$$

Applying the Cauchy–Schwarz inequality, we obtain for T_1 ,

$$(6.19) \quad T_1 = \int_0^T (\phi^{1/2} (\theta_c)_t, \phi^{1/2} \psi_c) dt \leq (\phi^*)^{1/2} \int_0^T \|(\theta_c)_t\| \|\phi^{1/2} \psi_c\| dt.$$

For the bound of T_2 we will use the L^2 -projection of \mathbf{u} onto the space of piecewise constant vectors $\Pi_0 \mathbf{u}$ satisfying

$$\forall E \in \mathcal{T}_h, \quad (\mathbf{u} - \Pi_0 \mathbf{u}, \mathbf{1})_E = 0, \quad \|\mathbf{u} - \Pi_0 \mathbf{u}\|_{0,p,E} \leq K h_E \|\mathbf{u}\|_{1,p,E}, \quad 1 \leq p \leq \infty.$$

Using (6.1), we have

$$(6.20) \quad \begin{aligned} T_2 &= - \int_0^T \sum_E (\theta_c \mathbf{u}, \nabla \psi_c)_E dt = \int_0^T \sum_E (\theta_c (\Pi_0 \mathbf{u} - \mathbf{u}), \nabla \psi_c)_E dt \\ &\leq K \|\mathbf{u}\|_{1,\infty} \int_0^T \sum_E h_E \|\theta_c\|_E \|\nabla \psi_c\|_E dt \leq K \|\mathbf{u}\|_{1,\infty} \int_0^T \sum_E \|\theta_c\|_E \|\psi_c\|_E dt \\ &\leq K \|\mathbf{u}\|_{1,\infty} \phi_*^{-1/2} \int_0^T \|\theta_c\| \|\phi^{1/2} \psi_c\| dt, \end{aligned}$$

where we used (6.7) for the second inequality. Handling T_4 is straightforward, using (5.11) with $\epsilon = 1/2$:

$$(6.21) \quad T_4 = \int_0^T \sum_E (\mathbf{D}^{-1} \theta_{\mathbf{z}}, \psi_{\mathbf{z}})_E dt \leq \int_0^T \|\mathbf{D}^{-1/2} \theta_{\mathbf{z}}\|^2 dt + \frac{1}{4} \int_0^T \|\mathbf{D}^{-1/2} \psi_{\mathbf{z}}\|^2 dt.$$

Using (6.4), we have for T_6 and T_7 ,

$$(6.22) \quad \begin{aligned} T_6 + T_7 &= \int_0^T \sum_E \left\{ (\nabla \cdot (\Pi c (\mathbf{u} - \mathbf{U})), \psi_c)_E - \frac{1}{2} (\Pi c \nabla \cdot (\mathbf{u} - \mathbf{U}), \psi_c)_E \right\} dt \\ &= \int_0^T \sum_E \left\{ (\nabla \Pi c \cdot (\mathbf{u} - \mathbf{U}), \psi_c)_E + \frac{1}{2} (\Pi c \nabla \cdot (\mathbf{u} - \mathbf{U}), \psi_c)_E \right\} dt \\ &\leq \phi_*^{-1/2} \int_0^T \sum_E (\|\nabla \Pi c\|_{0,\infty,E} \|\mathbf{u} - \mathbf{U}\|_E + \|\Pi c\|_{0,\infty,E} \|\nabla \cdot (\mathbf{u} - \mathbf{U})\|_E) \|\phi^{1/2} \psi_c\|_E dt \\ &\leq K \phi_*^{-1/2} \int_0^T \|c\|_{1,\infty} \|\mathbf{u} - \mathbf{U}\|_X \|\phi^{1/2} \psi_c\| dt. \end{aligned}$$

For T_8 , we have

$$\begin{aligned}
 (6.23) \quad T_8 &= \int_0^T \sum_E \langle ((\Pi c)^u - (\Pi c)^-)(\mathbf{u} - \mathbf{U}) \cdot \mathbf{n}_E, \psi_c^- \rangle_{\partial E \setminus \Gamma} dt \\
 &\leq \int_0^T \sum_E \|((\Pi c)^u - (\Pi c)^-)\|_{0,\infty,\partial E \setminus \Gamma} \|(\mathbf{u} - \mathbf{U}) \cdot \mathbf{n}_E\|_{\partial E \setminus \Gamma} \|\psi_c^-\|_{\partial E \setminus \Gamma} dt.
 \end{aligned}$$

Note that

$$\|((\Pi c)^u - (\Pi c)^-)\|_{0,\infty,\partial E} \leq \|((\Pi c)^u - c)\|_{0,\infty,\partial E} + \|c - (\Pi c)^-\|_{0,\infty,\partial E} \leq \|c - \Pi c\|_{0,\infty,\delta(E)},$$

where $\delta(E)$ is the union of all elements that share an edge (face) with E . For the second term on the right in (6.23), we have

$$\begin{aligned}
 \|(\mathbf{u} - \mathbf{U}) \cdot \mathbf{n}_e\|_e &\leq \|(\mathbf{u} - \Pi \mathbf{u}) \cdot \mathbf{n}_e\|_e + \|(\Pi \mathbf{u} - \mathbf{U}) \cdot \mathbf{n}_e\|_e \\
 &\leq K(\|(\mathbf{u} - \Pi \mathbf{u}) \cdot \mathbf{n}_e\|_e + h_E^{-1/2} \|\Pi \mathbf{u} - \mathbf{U}\|_E) \\
 &\leq K(\|(\mathbf{u} - \Pi \mathbf{u}) \cdot \mathbf{n}_e\|_e + h_E^{-1/2} \|\mathbf{u} - \Pi \mathbf{u}\|_E + h_E^{-1/2} \|\mathbf{u} - \mathbf{U}\|_E),
 \end{aligned}$$

where the second inequality follows from an application of (6.8). Therefore for T_8 we obtain, using (6.8) again,

$$\begin{aligned}
 (6.24) \quad T_8 &\leq K \int_0^T \|\theta_c\|_{0,\infty} \sum_E (\|(\mathbf{u} - \Pi \mathbf{u}) \cdot \mathbf{n}_E\|_{\partial E \setminus \Gamma} + h_E^{-1/2} \|\mathbf{u} - \Pi \mathbf{u}\|_E \\
 &\quad + h_E^{-1/2} \|\mathbf{u} - \mathbf{U}\|_E) h_E^{-1/2} \|\psi_c\|_E \\
 &\leq K \phi_*^{-1/2} \int_0^T \|c\|_{1,\infty} (h^{1/2} \|(\mathbf{u} - \Pi \mathbf{u}) \cdot \mathbf{n}\|_{\mathcal{E}_h} + \|\mathbf{u} - \Pi \mathbf{u}\| + \|\mathbf{u} - \mathbf{U}\|) \|\phi^{1/2} \psi_c\|,
 \end{aligned}$$

where $\|w\|_{\mathcal{E}_h} = (\sum_e \|w\|_e^2)^{1/2}$. Similarly, for T_9 we have

$$\langle \theta_c^u \mathbf{u}, [\psi_c] \rangle_e \leq K \phi_*^{-1/2} \|\mathbf{u} \cdot \mathbf{n}_e\|_{0,\infty,e} \|\theta_c^u\|_e h_E^{-1/2} \|\phi^{1/2} \psi_c\|_E,$$

and therefore,

$$(6.25) \quad T_9 \leq K \|\mathbf{u}\|_{0,\infty} \phi_*^{-1/2} \int_0^T h^{-1/2} \|\theta_c^u\|_{\mathcal{E}_h} \|\phi^{1/2} \psi_c\|.$$

Similarly,

$$(6.26) \quad T_{10} \leq K \phi_*^{-1/2} \int_0^T h^{-1/2} \|\overline{\theta}_c \cdot \mathbf{n}\|_{\mathcal{E}_h} \|\phi^{1/2} \psi_c\|$$

and

$$\begin{aligned}
 (6.27) \quad T_{11} &= \int_0^T \sum_e \langle \overline{\theta}_c, [\psi_{\mathbf{z}}] \rangle_e dt \\
 &\leq K(D^*)^{1/2} \int_0^T h^{-1/2} \|\overline{\theta}_c\|_{\mathcal{E}_h} \|\mathbf{D}^{-1/2} \psi_{\mathbf{z}}\| dt \\
 &\leq K^2 D^* \int_0^T h^{-1} \|\overline{\theta}_c\|_{\mathcal{E}_h}^2 dt + \frac{1}{4} \int_0^T \|\mathbf{D}^{-1/2} \psi_{\mathbf{z}}\|^2 dt,
 \end{aligned}$$

using (5.11) with $\epsilon = 1/2$ for the last inequality. In a similar way, we obtain

$$(6.28) \quad T_{12} \leq K \|\mathbf{u}\|_{0,\infty} \phi_*^{-1/2} \int_0^T h^{-1/2} \|\theta_c^-\|_{\Gamma_{out}} \|\phi^{1/2} \psi_c\| \, dt,$$

$$(6.29) \quad T_{13} \leq K D^* \int_0^T h^{-1} \|\theta_c^-\|_{\Gamma}^2 \, dt + \frac{1}{4} \int_0^T \|\mathbf{D}^{-1/2} \psi_{\mathbf{z}}\|^2 \, dt,$$

and

$$(6.30) \quad T_{14} \leq K \phi_*^{-1/2} \int_0^T \|c\|_{0,\infty,\Gamma} h^{-1/2} \|(\mathbf{u} - \mathbf{U}) \cdot \mathbf{n}\|_{\Gamma} \|\phi^{1/2} \psi_c\| \, dt.$$

A combination of (6.16)–(6.30), the use of Gronwall’s inequality for the term in (6.17), and an application of Lemma 5.1 imply

$$(6.31) \quad \begin{aligned} |||(\psi_c, \psi_{\mathbf{z}})||| \leq K \int_0^T & \left(\|\mathbf{D}^{-1/2} \theta_{\mathbf{z}}\| + h^{-1/2} \|\overline{\theta}_c\|_{\mathcal{E}_h} + h^{-1/2} \|\theta_c^-\|_{\Gamma} \right. \\ & + \|(\theta_c)_t\| + \|\theta_c\| + \|\mathbf{u} - \mathbf{U}\|_X + h^{1/2} \|(\mathbf{u} - \Pi \mathbf{u}) \cdot \mathbf{n}\|_{\mathcal{E}_h} \\ & + \|\mathbf{u} - \Pi \mathbf{u}\| + \|\mathbf{u} - \mathbf{U}\| + h^{-1/2} \|\theta_c^u\|_{\mathcal{E}_h} + h^{-1/2} \|\overline{\theta}_{\mathbf{z}} \cdot \mathbf{n}\|_{\mathcal{E}_h} \\ & \left. + h^{-1/2} \|\theta_c^-\|_{\Gamma_{out}} + h^{-1/2} \|(\mathbf{u} - \mathbf{U}) \cdot \mathbf{n}\|_{\Gamma} \right) dt, \end{aligned}$$

where $K = K(e^{LT})$. The above bound, combined with the velocity error bounds (3.3) and (3.4) and the approximation properties (6.4) and (6.6), implies the following convergence result.

THEOREM 6.1. *If the solution to the coupled system (2.1)–(2.14) is smooth enough, then the solution to the semidiscrete transport LDG method (4.10)–(4.12) satisfies*

$$(6.32) \quad |||(c - C, \mathbf{z} - \mathbf{Z})||| \leq K(h^k + h_1^{k_1} + h_2^{k_2+\beta} + h_2^{l_2+1}),$$

where $\beta = 1$ if $g_2 = 0$, and $\beta = 1/2$ otherwise.

7. Numerical results. In this section, we present results from several computational experiments. The first three confirm the theoretical convergence rates for problems with given analytical solutions, while the last two illustrate the behavior of the method for realistic problems of coupled surface–subsurface flows with contaminant transport. In all tests the computational domain is taken to be $\Omega = \Omega_1 \cup \Omega_2$, where $\Omega_1 = [0, 1] \times [\frac{1}{2}, 1]$ and $\Omega_2 = [0, 1] \times [0, \frac{1}{2}]$. For simplicity we have used

$$\mathbf{T}(\mathbf{u}_1, p_1) = -p_1 \mathbf{I} + \mu \nabla \mathbf{u}_1$$

in the Stokes equation in Ω_1 . The flow equations are solved via domain decomposition using the Taylor–Hood triangular finite elements in Ω_1 and the lowest order Raviart–Thomas rectangular finite elements in Ω_2 . In the LDG discretization of the transport equation, we chose $W_{h,E}$ to be the space of bilinear functions on E . With these choices,

$$k_1 = 2, \quad k_2 = l_2 = 0, \quad \text{and} \quad k = 1.$$

The grid for the Stokes discretization in Ω_1 is obtained by first partitioning the domain into rectangles and then dividing each rectangle along its diagonal into two triangles. The flow grids in Ω_1 and Ω_2 match on the interface. The LDG transport grid on Ω is the rectangular grid used for the flow discretization (on Ω_1 this is the grid before subdividing into triangles).

The computed Stokes–Darcy velocity \mathbf{U} is used in the transport scheme by first projecting it onto the space of piecewise bilinear functions on the transport grid. In the Stokes region the computed Taylor–Hood velocity vector is quadratic on each triangle, and it is simply evaluated at the vertices of each rectangle. In the Darcy region the velocity vector at each vertex is recovered by combining the Raviart–Thomas normal velocities on the two edges forming the vertex.

Remark 7.1. The choice of rectangular elements in the Darcy domain was motivated by the superior accuracy and efficiency (including velocity superconvergence) of the MFE method on rectangles, compared to simplicial elements. There exist extensions of the MFE method to quadrilaterals and hexahedra that exhibit accuracy and efficiency similar to the rectangular case. However, since the theory in this paper is presented only for affine elements, we limit the numerical results to rectangular elements in the Darcy domain.

7.1. Convergence tests. In the three convergence tests we use a second-order Runge–Kutta method to discretize the transport equation in time. The final time is $T = 2$, and the time step is $\Delta t = 10^{-3}$, all numbers being dimensionless. The time step is chosen small enough so that the time discretization error is smaller than the spatial discretization error even for the finest grids used. In the convergence tests with nonzero diffusion we take $\mathbf{D} = 10^{-3} \mathbf{I}$, where \mathbf{I} is the identity matrix. To handle the purely hyperbolic case $\mathbf{D} = 0$, we introduce an auxiliary variable $\tilde{\mathbf{z}} = -\nabla c$ and set $\mathbf{z} = \mathbf{D}\tilde{\mathbf{z}}$, following an approach from [2] for MFE methods for elliptic problems. The LDG analysis for this formulation has been carried out in [13]. In all convergence tests we take $\phi = 1$.

The true solution of the transport equation for all three tests is

$$c(x, y, t) = t(\cos(\pi x) + \cos(\pi y))/\pi.$$

It is chosen to satisfy the outflow boundary condition (2.14) on $\partial\Omega$. The source function s is obtained by plugging into (2.11) the true solution functions for the concentration and the velocity specified below. The sign of the normal component of the true velocity determines whether the inflow or the outflow boundary condition is used for the transport equation. The initial condition function c^0 and the inflow condition function c_{in} are obtained by evaluating the true concentration at $t = 0$ and $\mathbf{x} \in \Gamma_{in}$, respectively.

In Test 1 the velocity field is chosen to be smooth across the interface:

$$\begin{aligned} \mathbf{u}_1 = \mathbf{u}_2 &= \begin{bmatrix} \sin\left(\frac{x}{G} + \omega\right)e^{y/G} \\ -\cos\left(\frac{x}{G} + \omega\right)e^{y/G} \end{bmatrix}, \\ p_1 &= \left(\frac{G}{K} - \frac{\mu}{G}\right) \cos\left(\frac{x}{G} + \omega\right) e^{1/(2G)} + y - 0.5, \\ p_2 &= \frac{G}{K} \cos\left(\frac{x}{G} + \omega\right) e^{y/G}, \end{aligned}$$

where

$$\mu = 0.1, \quad K = 1, \quad \alpha = 0.5, \quad G = \frac{\sqrt{\mu K}}{\alpha}, \quad \text{and } \omega = 1.05.$$

The velocity \mathbf{u}_1 in the Stokes region is divergence free. The right-hand sides \mathbf{f}_1 and \mathbf{f}_2 for the Stokes–Darcy flow system are obtained by plugging the above functions into (2.1) and (2.4), respectively. For the Stokes region, the velocity \mathbf{u}_1 is specified on the left and top boundaries, and the normal and tangential stresses $\mathbf{n}_1 \cdot \mathbf{T} \cdot \mathbf{n}_1$ and $\mathbf{n}_1 \cdot \mathbf{T} \cdot \boldsymbol{\tau}_1$ are specified on the right boundary. In the Darcy region, the normal velocity $\mathbf{u}_2 \cdot \mathbf{n}_2$ is specified on the left boundary and the pressure is specified on the bottom and right boundaries.

In test 2 the velocity field is continuous, but not smooth, across the interface between the two subdomains:

$$\begin{aligned} \mathbf{u}_1 &= \begin{bmatrix} (2-x)(1.5-y)(y-\xi) \\ -\frac{y^3}{3} + \frac{y^2}{2}(\xi+1.5) - 1.5\xi y - 0.5 \end{bmatrix}, \\ \mathbf{u}_2 &= \begin{bmatrix} (2-x)(0.5-\xi) \\ \chi(y+0.5) \end{bmatrix}, \\ p_1 &= \frac{1}{K} \left(\frac{x^2}{2} - 2x \right) (0.5-\xi) - \frac{11\chi}{8K} + \mu(0.5-\xi) + y - 0.5, \\ p_2 &= \frac{1}{K} \left(\frac{x^2}{2} - 2x \right) (0.5-\xi) + \frac{\chi}{K} \left(-\frac{y^2+y}{2} - 1 \right), \end{aligned}$$

where

$$\xi = \frac{1-G}{2(1+G)}, \quad \chi = \frac{-30\xi-17}{48},$$

and $\mu, K, \alpha,$ and G are defined as in test 1.

In test 3 the normal velocity is continuous, but the tangential velocity is discontinuous across the interface:

$$\begin{aligned} \mathbf{u}_1 &= \begin{bmatrix} (2-x)(1.5-y)(y-\xi) \\ -\frac{y^3}{3} + \frac{y^2}{2}(\xi+1.5) - 1.5\xi y - 0.5 + \sin(\omega x) \end{bmatrix}, \\ \mathbf{u}_2 &= \begin{bmatrix} \omega \cos(\omega x)y \\ \chi(y+0.5) + \sin(\omega x) \end{bmatrix}, \\ p_1 &= -\frac{\sin(\omega x) + \chi}{2K} + \mu(0.5-\xi) + \cos(\pi y), \\ p_2 &= -\frac{\chi}{K} \frac{(y+0.5)^2}{2} - \frac{\sin(\omega x)y}{K}, \end{aligned}$$

where $\omega = 6$ and the other parameters are defined as in test 2.

In all three tests, the solutions are designed to satisfy the interface conditions (2.8)–(2.10).

The computed velocity field in test 3 is shown in Figure 7.1. Note that the flow domain decomposition scheme correctly imposes continuity of the normal velocity but allows for discontinuous tangential velocity across the interface.

The convergence rates for the transport equation are studied by solving the coupled flow-transport system on several levels of grid refinement. We test convergence with and without diffusion. The numerical errors and convergence rates for the three

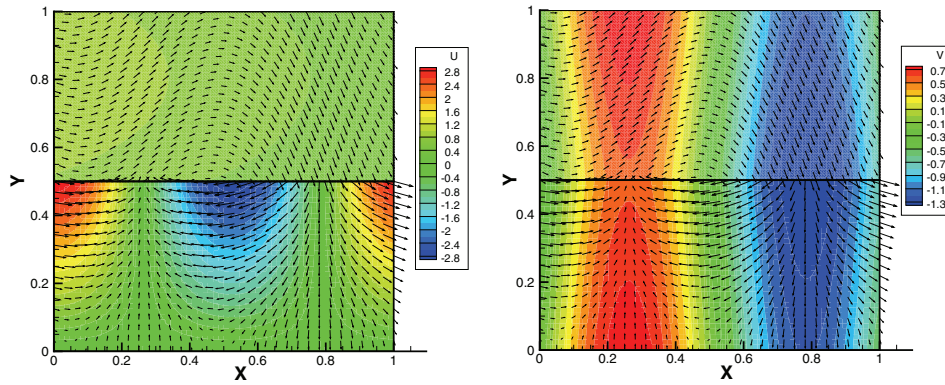


FIG. 7.1. Computed velocity field in test 3: discontinuous tangential velocity. Left: horizontal velocity; right: vertical velocity.

TABLE 7.1
Computed numerical errors and convergence rates for test 1: smooth velocity.

mesh	$D = 10^{-3} \mathbf{I}$				$D = 0$	
	$\ c - C\ _{L^\infty(L^2)}$	rate	$\ \mathbf{z} - \mathbf{Z}\ _{L^2(L^2)}$	rate	$\ c - C\ _{L^\infty(L^2)}$	rate
4x4	5.50e-02		5.31e-04		5.54e-02	
8x8	1.44e-02	1.93	2.39e-04	1.15	1.46e-02	1.93
16x16	3.75e-03	1.95	1.09e-04	1.13	3.81e-03	1.93
32x32	9.84e-04	1.93	5.09e-05	1.10	1.01e-03	1.92
64x64	2.60e-04	1.92	2.43e-05	1.07	2.71e-04	1.90

TABLE 7.2
Computed numerical errors and convergence rates for test 2: continuous velocity.

mesh	$D = 10^{-3} \mathbf{I}$				$D = 0$	
	$\ c - C\ _{L^\infty(L^2)}$	rate	$\ \mathbf{z} - \mathbf{Z}\ _{L^2(L^2)}$	rate	$\ c - C\ _{L^\infty(L^2)}$	rate
4x4	5.57e-02		4.33e-04		5.63e-02	
8x8	1.39e-02	2.00	2.01e-04	1.10	1.41e-02	2.00
16x16	3.48e-03	2.00	9.62e-05	1.07	3.51e-03	2.00
32x32	8.69e-04	2.00	4.70e-05	1.03	8.77e-04	2.00
64x64	2.17e-04	2.00	2.33e-05	1.01	2.19e-04	2.00

TABLE 7.3
Computed numerical errors and convergence rates for test 3: discontinuous tangential velocity.

mesh	$D = 10^{-3} \mathbf{I}$				$D = 0$	
	$\ c - C\ _{L^\infty(L^2)}$	rate	$\ \mathbf{z} - \mathbf{Z}\ _{L^2(L^2)}$	rate	$\ c - C\ _{L^\infty(L^2)}$	rate
4x4	1.99e+00		8.95e-03		2.07e+00	
8x8	3.27e-01	2.60	2.71e-03	1.72	3.39e-01	2.61
16x16	8.48e-02	1.95	1.20e-03	1.18	9.04e-02	1.91
32x32	2.23e-02	1.93	5.33e-04	1.17	2.59e-02	1.80
64x64	5.60e-03	2.00	1.77e-04	1.59	7.76e-03	1.74

tests are reported in Tables 7.1, 7.2, and 7.3. In all three cases we observe experimental convergence of order $O(h^2)$ for the concentration error in $L^\infty(0, T; L^2(\Omega))$ and approaching $O(h)$ for the diffusive flux error in $L^2(0, T; L^2(\Omega))$. Our theoretical results predict $O(h)$ for both variables. Similar second-order convergence for

the concentration has been observed numerically in the literature for the stand-alone transport equation; see, e.g., [1]. Higher order convergence $O(h^{k+1})$ for the $L^2(0, T; L^2(\Omega))$ error of the concentration has been obtained theoretically by adding penalty terms [18, 9]. In our case there are additional terms contributing to the transport numerical error that are coming from the discretization error in the Stokes–Darcy velocity. For our particular choice of flow discretization these terms are $O(h^2)$ from Stokes and $O(h)$ from Darcy. The observed second-order convergence of the concentration may be due to the superconvergence of the Raviart–Thomas velocity at the edge midpoints, which are used to obtain the bilinear velocity for the transport scheme. Further theoretical investigation of this phenomenon will be a topic of future work.

7.2. Contaminant transport examples. We present two simulations of coupled surface and subsurface flow and contaminant transport. The Stokes region Ω_1 represents a lake or a river, which interacts with an aquifer occupying the Darcy region Ω_2 . The porous medium is heterogeneous with permeability varying approximately two orders of magnitude; see Figure 7.2.

In both examples, we use the following flow boundary conditions. In the Stokes region we set parabolic inflow on the left boundary, no normal flow and zero tangential stress on the top boundary, and zero normal and tangential stress on the right (out-flow) boundary. In the Darcy region we set no flow on the left and right boundaries and specify pressure on the bottom boundary to simulate a gravity force. The computed velocity field for the two simulations is shown in Figure 7.3.

In example 1, a plume of contaminant present at the initial time in the surface water region is transported into the porous media. In example 2, inflow of the contaminant is specified on part of the left boundary in the surface water region. The contaminant front eventually reaches and penetrates into the subsurface water region.

The diffusion tensor is chosen to be $\mathbf{D}_{\Omega_1} = 10^{-6}\mathbf{I}$ in the Stokes region and

$$\mathbf{D}_{\Omega_2} = \phi d_m \mathbf{I} + d_l |\mathbf{u}| \mathbf{T} + d_t |\mathbf{u}| (\mathbf{I} - \mathbf{T})$$

in the Darcy region, where $\mathbf{T} = \frac{\mathbf{u}\mathbf{u}}{|\mathbf{u}|^2}$ and the parameters values are $\phi = 0.4, d_m = d_l = d_t = 10^{-5}$. Here, d_m represents molecular diffusion, while d_l and d_t represent longitudinal and transverse dispersion, respectively. The simulations were carried out using the forward Euler method for the temporal discretization with $\Delta t = 10^{-3}$ on a square 80×80 mesh.

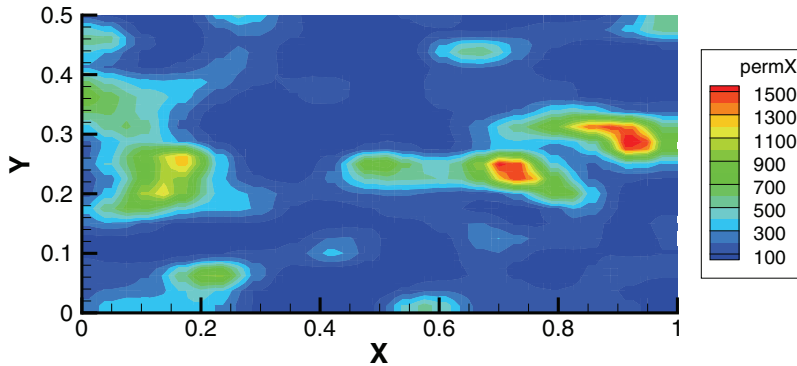


FIG. 7.2. Permeability of the porous medium in the contaminant transport examples.

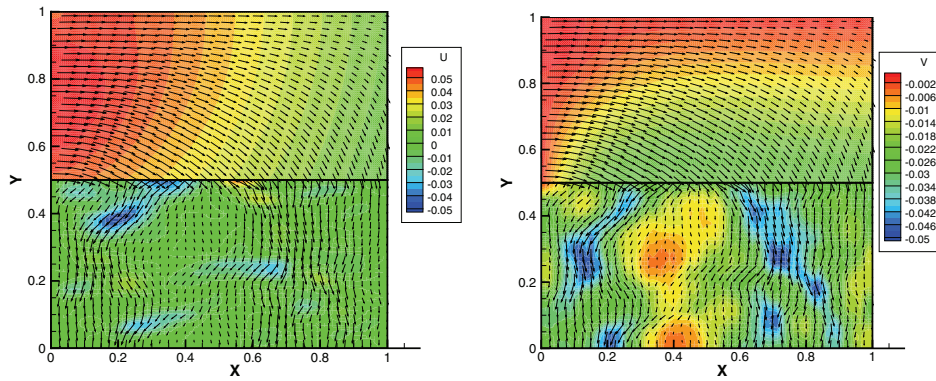


FIG. 7.3. Computed velocity field in the contaminant transport examples. Left: horizontal velocity; right: vertical velocity.

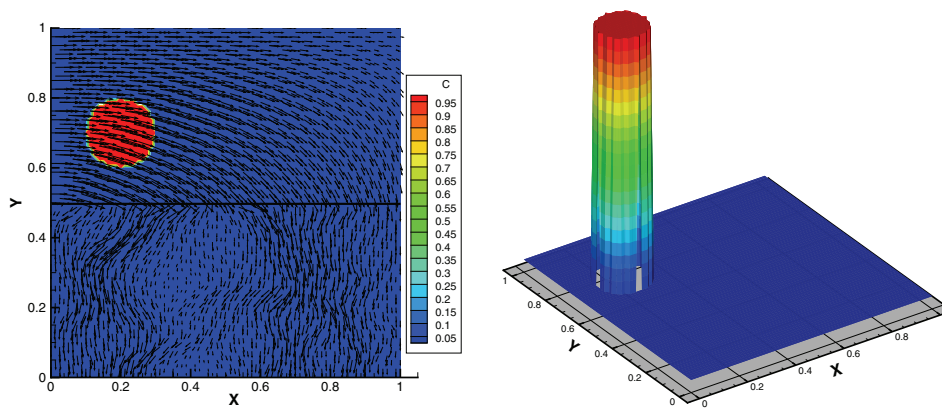


FIG. 7.4. Initial plume, $t=0.0$. The arrows represent the computed Stokes–Darcy velocity.

Due to the discontinuity in the initial (example 1) or boundary (example 2) conditions and small diffusion/dispersion values, the simulations exhibit steep concentration gradients. In such cases a slope limiting procedure is often employed in the LDG scheme to remove oscillations [14, 1]. Our approach is based on [23]. For each element, local extremum is avoided by comparing the averages of the concentration over the edges with the averages of the concentration over the neighboring elements. The concentration values at the vertices are reconstructed by imposing mass conservation on the element. The procedure is equivalent to an optimization problem with parametrized equality constraints. Tighter constraints introduce more numerical diffusion and lead to a smoother solution. More relaxed constraints allow for better approximation of propagating sharp fronts.

Plots of the contaminant concentration at various simulation times are shown in Figures 7.4–7.8 for example 1 and Figures 7.9–7.11 for example 2. Both two- and three-dimensional views are included for better illustration of the steep concentration gradients.

In example 1, the plume stays compact while in the surface water region. When it reaches the groundwater region, it starts to spread due to the heterogeneity of the porous media. The discontinuity in the tangential velocity along the interface causes

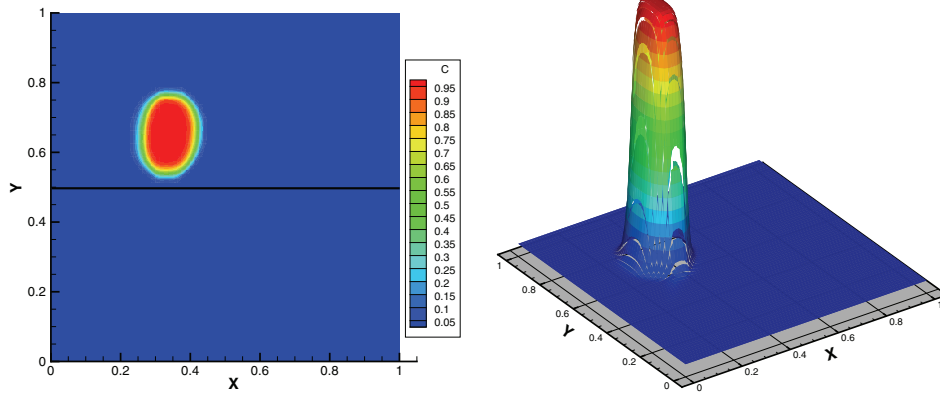


FIG. 7.5. The plume at early time is confined to the surface water region, $t=3.0$.

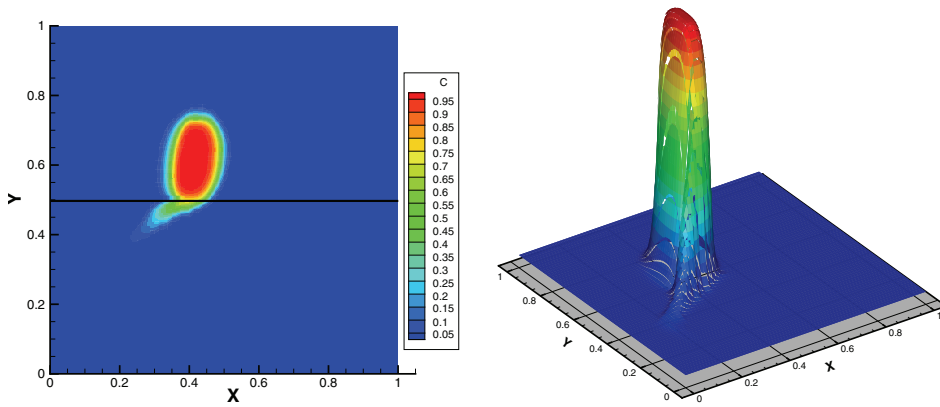


FIG. 7.6. The plume penetrates the porous medium, $t=5.0$.

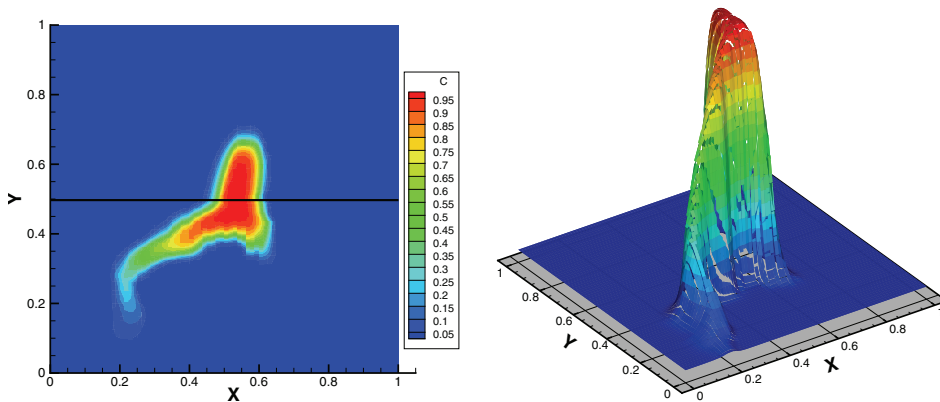


FIG. 7.7. The plume spreads through the porous medium, $t=9.0$.

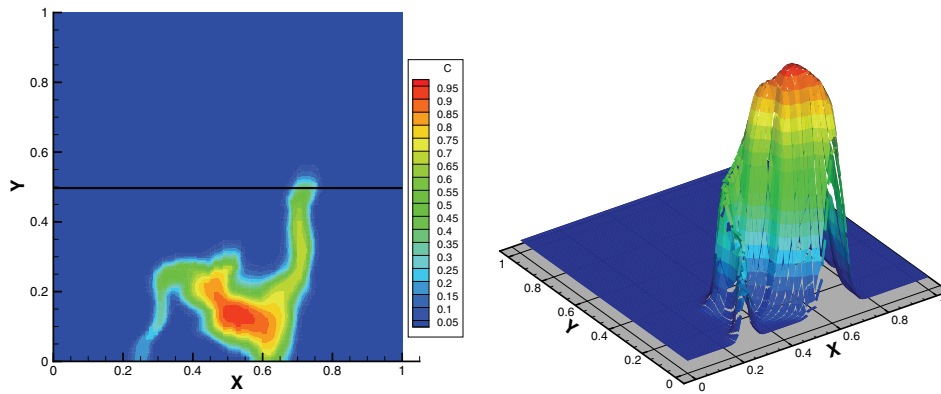


FIG. 7.8. Most of the plume has been transported to the porous medium, $t=16.0$.

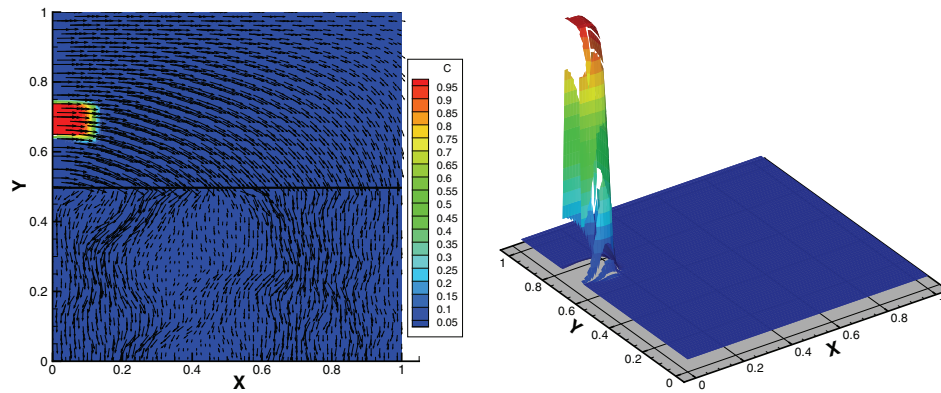


FIG. 7.9. The front enters the surface water region, $t=2.0$. The arrows represent the computed Stokes–Darcy velocity.

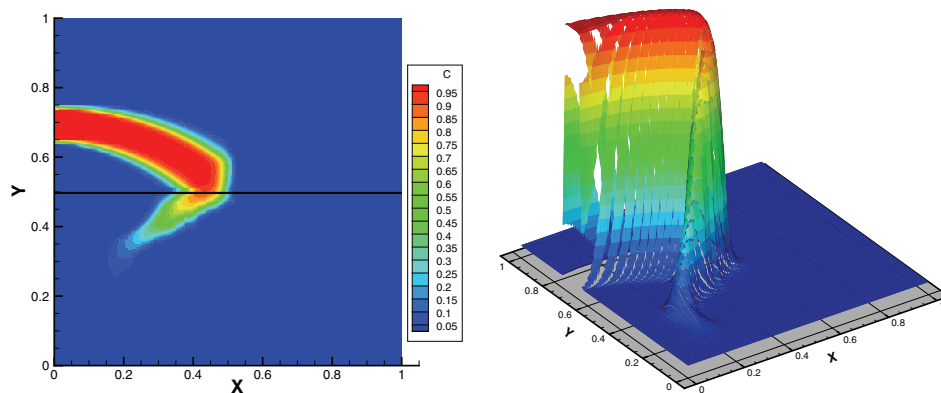


FIG. 7.10. The front reaches the porous medium, $t=11.0$.

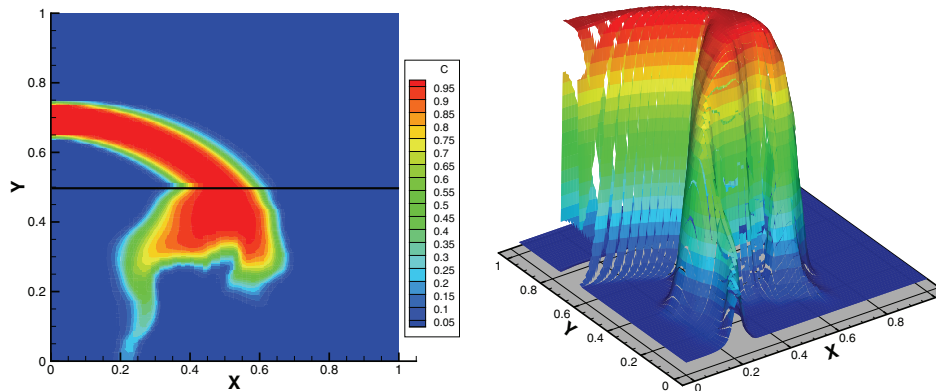


FIG. 7.11. The front propagates inside the porous medium, $t=17.0$.

some of the contaminant to lag behind and even move in the opposite direction. Similar behavior is observed in example 2, where the contaminant front maintains a relatively flat interface in the surface water region and spreads nonuniformly in the porous media. In both cases, the LDG method with slope limiter preserves sharp discontinuities in the concentration without numerical oscillations.

REFERENCES

- [1] V. AIZINGER, C. N. DAWSON, B. COCKBURN, AND P. CASTILLO, *The local discontinuous Galerkin method for contaminant transport*, *Adv. Water Resour.*, 24 (2000), pp. 73–87.
- [2] T. ARBOGAST, M. F. WHEELER, AND I. YOTOV, *Mixed finite elements for elliptic problems with tensor coefficients as cell-centered finite differences*, *SIAM J. Numer. Anal.*, 34 (1997), pp. 828–852.
- [3] D. N. ARNOLD, F. BREZZI, AND M. FORTIN, *A stable finite element for the Stokes equations*, *Calcolo*, 21 (1984), pp. 337–344.
- [4] D. ARNOLD, *An interior penalty finite element method with discontinuous elements*, *SIAM J. Numer. Anal.*, 19 (1982), pp. 742–760.
- [5] G. BEAVERS AND D. JOSEPH, *Boundary conditions at a naturally impermeable wall*, *J. Fluid. Mech.*, 30 (1967), pp. 197–207.
- [6] F. BREZZI, J. DOUGLAS, JR., R. DURÀN, AND M. FORTIN, *Mixed finite elements for second order elliptic problems in three variables*, *Numer. Math.*, 51 (1987), pp. 237–250.
- [7] F. BREZZI, J. DOUGLAS, JR., M. FORTIN, AND L. D. MARINI, *Efficient rectangular mixed finite elements in two and three space variables*, *RAIRO Modèl. Math. Anal. Numèr.*, 21 (1987), pp. 581–604.
- [8] F. BREZZI, J. DOUGLAS, JR., AND L. D. MARINI, *Two families of mixed elements for second order elliptic problems*, *Numer. Math.*, 88 (1985), pp. 217–235.
- [9] P. CASTILLO, B. COCKBURN, I. PERUGIA, AND D. SCHÖTZAU, *An a priori error analysis of the local discontinuous Galerkin method for elliptic problems*, *SIAM J. Numer. Anal.*, 38 (2000), pp. 1676–1706.
- [10] P. CASTILLO, B. COCKBURN, D. SCHÖTZAU, AND C. SCHWAB, *Optimal a priori error estimates for the hp-version of the local discontinuous Galerkin method for convection-diffusion problems*, *Math. Comp.*, 71 (2002), pp. 455–478.
- [11] Z. CHEN AND J. DOUGLAS, JR., *Prismatic mixed finite elements for second order elliptic problems*, *Calcolo*, 26 (1989), pp. 135–148.
- [12] P. CIARLET, *The Finite Element Method for Elliptic Problems*, North-Holland, Amsterdam, 1978.
- [13] B. COCKBURN AND C. DAWSON, *Some extensions of the local discontinuous Galerkin method for convection-diffusion equations in multidimensions*, in *The Mathematics of Finite Elements and Applications, X, MAFELAP 1999* (Uxbridge), Elsevier, Oxford, 2000, pp. 225–238.

- [14] B. COCKBURN, S. HOU, AND C.-W. SHU, *The Runge-Kutta local projection discontinuous Galerkin finite element method for conservation laws. IV. The multidimensional case*, Math. Comp., 54 (1990), pp. 545–581.
- [15] B. COCKBURN AND C.-W. SHU, *The local discontinuous Galerkin method for time-dependent convection-diffusion systems*, SIAM J. Numer. Anal., 35 (1998), pp. 2440–2463.
- [16] B. COCKBURN AND C.-W. SHU, *Runge-Kutta discontinuous Galerkin methods for convection-dominated problems*, J. Sci. Comput., 16 (2001), pp. 173–261.
- [17] M. CROUZEIX AND P.-A. RAVIART, *Conforming and nonconforming finite element methods for solving the stationary Stokes equations. I*, Rev. Française Automat. Informat. Recherche Opérationnelle Sér. Rouge, 7 (1973), pp. 33–75.
- [18] C. DAWSON AND J. PROFT, *A priori error estimates for interior penalty versions of the local discontinuous Galerkin method applied to transport equations*, Numer. Methods Partial Differential Equations, 17 (2001), pp. 545–564.
- [19] C. DAWSON, S. SUN, AND M. F. WHEELER, *Compatible algorithms for coupled flow and transport*, Comput. Methods Appl. Mech. Engrg., 193 (2004), pp. 2565–2580.
- [20] C. DAWSON, *Conservative, shock-capturing transport methods with nonconservative velocity approximations*, Comput. Geosci., 3 (1999), pp. 205–227.
- [21] M. DISCACCIATI, E. MIGLIO, AND A. QUARTERONI, *Mathematical and numerical models for coupling surface and groundwater flows*, Appl. Numer. Math., 43 (2002), pp. 57–74.
- [22] J. GALVIS AND M. SARKIS, *Non-matching mortar discretization analysis for the coupling Stokes-Darcy equations*, Electron. Trans. Numer. Anal., 26 (2007), pp. 350–384.
- [23] H. HOTEIT, P. ACKERER, R. MOSE, J. ERHEL, AND B. PHILIPPE, *New two-dimensional slope limiters for discontinuous Galerkin methods on arbitrary meshes*, Internat. J. Numer. Methods Engrg., 61 (2004), pp. 2566–2593.
- [24] W. LAYTON, F. SCHIEWECK, AND I. YOTOV, *Coupling fluid flow with porous media flow*, SIAM J. Numer. Anal., 40 (2003), pp. 2195–2218.
- [25] K. A. MARDAL, X.-C. TAI, AND R. WINTHER, *A robust finite element method for Darcy-Stokes flow*, SIAM J. Numer. Anal., 40 (2002), pp. 1605–1631.
- [26] J. C. NEDELEC, *Mixed finite elements in \mathbf{R}^3* , Numer. Math., 35 (1980), pp. 315–341.
- [27] R. A. RAVIART AND J. M. THOMAS, *A Mixed Finite Element Method for 2nd Order Elliptic Problems*, in Mathematical Aspects of the Finite Element Method, Lecture Notes in Math. 606, Springer-Verlag, New York, 1977, pp. 292–315.
- [28] B. RIVIÈRE AND I. YOTOV, *Locally conservative coupling of Stokes and Darcy flows*, SIAM J. Numer. Anal., 42 (2005), pp. 1959–1977.
- [29] P. SAFFMAN, *On the boundary condition at the surface of a porous media*, Stud. Appl. Math., 50 (1971), pp. 93–101.
- [30] S. SUN AND M. F. WHEELER, *Discontinuous Galerkin methods for coupled flow and reactive transport problems*, Appl. Numer. Math., 52 (2005), pp. 273–298.
- [31] S. SUN AND M. F. WHEELER, *Symmetric and nonsymmetric discontinuous Galerkin methods for reactive transport in porous media*, SIAM J. Numer. Anal., 43 (2005), pp. 195–219.
- [32] C. TAYLOR AND P. HOOD, *A numerical solution of the Navier-Stokes equations using the finite element technique*, Internat. J. Comput. & Fluids, 1 (1973), pp. 73–100.